CONF-9106158--7

E. FRICTIONAL PROCESSES AND NUCLEAR DISASSEMBLY IN VERY-HEAVY-ION COLLISIONS IN THE FERMI ENERGY REGIME*

W.U. Schröder

Department of Chemistry and NSRL, University of Rochester, Rochester, New York 14627, USA

CONF-9106158--7

DE92 000823

ABSTRACT

Exclusive measurements of charged products and neutrons were performed for the reactions ^{197}Au + (29 MeV/u) ^{208}Pb and ^{209}Bi + (28.2 MeV/u) ^{136}Xe. The multiplicities of neutrons and charged particles are found to indicate collision impact parameters with different sensitivities. Characteristic correlations observed between massive products and light particles suggest the dominance of the damped-reaction mechanism in the Fermi energy domain. For central collisions, massive fragments are no longer observed, and a considerable fraction of the mass of the system is found disassembled into light particles and clusters.

1. INTRODUCTION

Over the past one or two decades, considerable progress has been made[1-3] in developing a quantitative understanding of the dynamics of complex nuclear reactions occurring at bombarding energies of up to about 10 MeV per nucleon. In this low-energy domain, quasi-elastic, damped,[1] and fusion-like processes[2,3] are known to account for most of the reaction cross section. Except for the smallest impact parameters leading to fusion-evaporation in light to medium-heavy systems, the collisions are essentially of a binary nature, with only two massive fragments in the exit channel. The collision

*An abreviated version of this article was presented as and invited paper at the Fourth International Conference on Nucleus-Nucleus Collisions in Kanazawa, Japan, June 10-14, 1991.

MASTER

FG02-88ER40414

trajectories, such as sketched in the upper portion of Fig. 1, are determined by the balance of conservative and dissipative interaction forces generated by the superposition of the mean fields of the interacting nuclei. This balance shifts in a predictable manner with mass asymmetry of the projectile-target system, the incident energy, and the collision impact parameter. Seemingly different phenomena such as Coulomb focussing (Fig. 1, top left) and orbiting (top right) can be explained[1] with the same set of interaction forces. In addition, the microscopic mechanism responsible for the nucleus-nucleus interaction forces at low bombarding energies are found[1,4,5] to give rise to a host of transport phenomena, redistributing the mass, charge, energy and angular momentum of the interacting system. Because of the impressive predictive power of models[4-6] considering transport induced by the exchange of independent nucleons between the constituents of the transient dinuclear system,[1] this latter process is generally thought to represent the dominant microscopic mechanism underlying the complex low-energy nuclear reaction phenomenology.

Essential determinants of mean-field reaction dynamics are a long mean free path of nucleons in a relatively cold dinuclear system, the unimportance of nucleonic correlations, and a collective motion that is slow enough for a continuous reestablishment of the mean nuclear field and of the intrinsic equilibrium within each nucleus to occur along a collision trajectory. This latter condition does not imply an overall equilibration of the dinuclear system, rarely found in damped reactions even at low energies.[7] Mean-field effects are expected to fade away slowly at bombarding or excitation energies per nucleon that are comparable to the nucleonic Fermi energy of $T_F \approx 37$ MeV. While it seems difficult to produce equilibrated nuclei with nucleon energy or momentum distributions much different from those of a degenerate Fermi gas, bombarding energies per nucleon of the order of T_F are readily available from modern accelerators. One, hence, expects a change in reaction phenomena to become observable at bombarding energies per nucleon approaching this "Fermi energy regime".

SCHEMATIC REACTION SCENARIOS

Low–Energy Domain

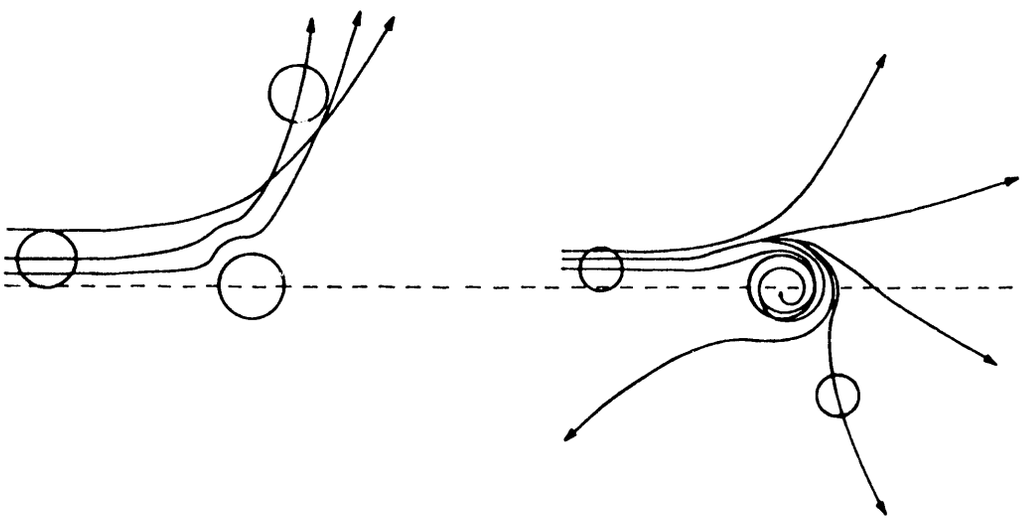

High–Energy Domain

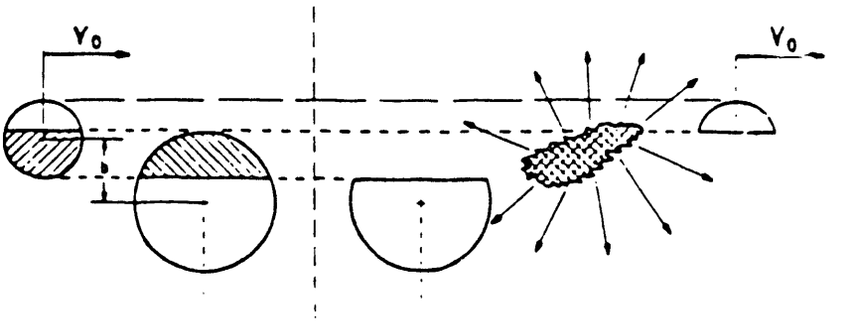

Figure 1

The nature of the mechanisms that take over in this energy domain and their experimental signatures represent topics of active current research.[8-18] On the one hand, one expects the onset of processes that are more fully developed at much higher energies such as fragmentation or participant-spectator mechanisms.[19-22] For example, in the bottom part of Fig. 1, a scenario[18] is depicted schematically, in which a hot participant zone is created along with relatively cold projectile and target spectators. On the other hand, completely new reaction mechanisms such as multifragmentation and vaporization have been postulated also,[10-18] based on the inherent instability developed[23,24] by a hot nuclear system. It is, therefore, an important goal of experiments to investigate the limiting excitation energy per nucleon that a nucleus can sustain and to explore efficient methods to produce such very hot nuclear systems.

Reaction features such as energy and mass distributions of light products from medium-energy reactions have, in the past, often been attributed[25-28] to fragmentation or participant-spectator processes, rather than to damped interactions known[1] from lower energies. However, these features can, on first sight, be quite deceptive and still be compatible with a primary damped reaction mechanism mediated by nucleon exchange (NEM), followed by the sequential decay of the hot primary fragments. It seems, hence, important to establish the range in bombarding energy and impact parameter over which the transition from the low-energy reaction mechanisms to intermediate-energy dynamics occurs.

Therefore, the strategy followed in the work reported on here was to explore to what extent dissipative reaction features characteristic of the low-energy regime are still found at bombarding energies of the order of 30 MeV/u. Of particular interest are correlations between the properties of projectile-like (PLF) and target-like (TLF) reaction products, as well as their dependence on the kinetic energy dissipated in a reaction. At low bombarding energies, the latter observable provides[1] a measure of impact parameter and reaction time. It is plausible that also in the medium-energy domain, the amount of energy

dissipated will be relatively small for gentle, peripheral collisions, and will increase with decreasing impact parameter.

In the work presented here, the symmetric and asymmetric heavy systems $^{197}Au + ^{208}Pb$ and $^{209}Bi + ^{136}Xe$ were chosen for study at 29 MeV/u and 28.2 MeV/u, respectively. For such heavy reaction systems that have just become accessible experimentally, reaction mechanisms are expected[1] to be more uniform than for light systems and should develop smoothly over a large range of impact parameters. In addition, interactions of heavier systems may lead[29,30] to hotter nuclei, since a given amount of energy available for intrinsic excitation can be supplied at a lower relative velocity of the reaction partners. As will be discussed in the following section, a lower approach speed is expected to reduce the amount of energy carried away instantaneously[31] by fast nonequilibrium particles.

The basis for and implementation of experimental methods employed in the present studies will be discussed in the following section. Experimental results will be presented in Section 3, along with a qualitative interpretation of the dissipative features in these reactions. Section 4 contains a summary.

2. CALORIMETRIC STUDIES OF ENERGY DISSIPATION

2.1. General Considerations

The interpretation of low-energy damped reactions has benefitted greatly[1] from the observation that the degree of energy damping in a collision is strongly correlated with impact parameter and interaction time. For these low-energy binary collisions, the loss of (total kinetic) energy, $(TK)E_{Loss}$, can be deduced already from the properties of one of the massive reaction products. Usually measured are those of the fast-moving projectile-like fragment (PLF). In Fig. 2, energy loss distributions measured for four heavy-ion reactions[32] are reproduced. The common features of these distributions are a shoulder at small energy losses, associated with quasi-elastic or peripheral reactions, and a broader distribution peaked at comparatively much larger energy losses. The arrows in Fig. 2

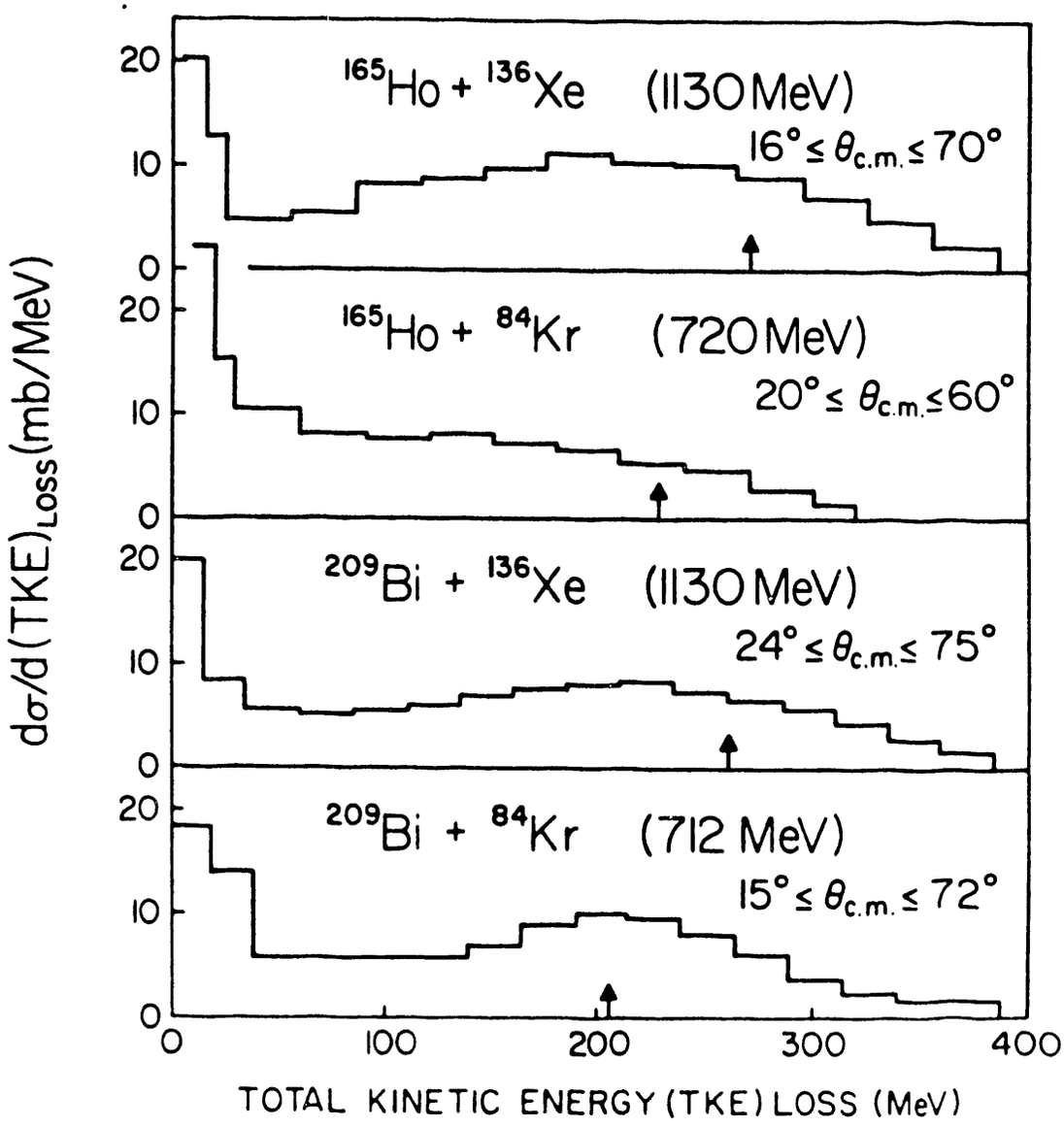
^{165}Ho + ^{136}Xe (1130 MeV)
16° ≤ θc.m. ≤ 70°
^{165}Ho + ^{84}Kr (720 MeV)
20° ≤ θc.m. ≤ 60°
^{209}Bi + ^{136}Xe (1130 MeV)
24° ≤ θc.m. ≤ 75°
^{209}Bi + ^{84}Kr (712 MeV)
15° ≤ θc.m. ≤ 72°
dσ/d(TKE)Loss (mb/MeV)
TOTAL KINETIC ENERGY (TKE) LOSS (MeV)
0
10
20
100
200
300
400

Figure 2

indicate the amounts E_{cm} of relative kinetic energy available in the entrance channel. Energy losses much larger than E_o must then correspond to scission of a highly elongated intermediate dinuclear system. Cross sections diminish exponentially for final kinetic energies at or below the kinetic energies,[33] E_f, for (asymmetric) fission. Hence, in low-energy binary collisions, the dissipated kinetic energy E_{Loss} is bounded in the range $0 \leq E_{Loss} \leq (E_{cm} - E_f)$.

At these low bombarding energies, the kinetic energy of relative motion dissipated in a collision is found to be converted almost entirely into excitation energy of the intermediate dinuclear system, as deduced[1,7,31] from measurements of particles (dominantly neutrons) evaporated in flight from the hot primary PLF and TLF. For most of the reaction cross section, the dissipated energy divides approximately equally[34-39] between PLF and TLF. This property gives rise to very characteristic correlations between the total amount of dissipated energy, E_{Loss}, the total intrinsic excitation energy E^*_{tot}, the excitation energies E^*_{PLF} and E^*_{TLF}, of PLF and TLF reaction partners, respectively, and their final laboratory kinetic energies. For example, a determination of the excitation energy of the slow-moving TLF will also determine the laboratory kinetic energy of the PLF, at any given angle. Because of the connection between energy loss and impact parameter or interaction time,[40] the same observable (for the TLF) correlates strongly with the properties of the PLF mass and charge distributions. The TLF excitation energy will also be related to the abundances and energy spectra of the particles evaporated from the PLF. These are correlations that can be utilized to investigate the primary reaction mechanism, even in cases where primary reaction fragments do not survive the subsequent deexcitation processes.

The methods employed in this work to deduce the total amount of dissipated energy are based on a measurement of neutrons and light charged particles (lcp) associated with a range of more massive charged reaction products. In the case of sequential emission of such particles from fragments in flight, the angle-energy emission patterns of these particles

allow for a determination of properties of the emitting source fragment. Due to the kinematical focussing of the sequentially emitted particles, source velocity vector and temperature can be deduced. The experimental results become more difficult to interpret in the presence of fast, nonequilibrium emission processes.

Nonequilibrium particles, emitted prior to the formation or equilibration of the primary reaction fragments, on the other hand, will reflect the dynamical conditions existing at early stages of the reaction. The emission patterns of such "jet" particles will be determined by the momentum transfer to TLF and PLF, respectively, for jet particles emitted into the forward and backward hemisphere, respectively, Since the emission patterns of such fast particles undoubtedly change continuously with the dynamics of a heavy-ion collision, there is, conceptionally, no unique physical source emitting these particles. However, partially due to the limited accuracy of the data on nonequilibrium particles, it is usually possible to describe their emission patterns in terms of isotropic emission from a hypothetical, effective emission source. Average velocities of such effective sources range between 0.5 and 0.8 of the velocity of the beam.

Nonequilibrium particle emission appears to gain importance with increasing relative kinetic energy per nucleon above the barrier.[31,41,42] For the nearly central collisions leading to fusion in reactions induced by light ions,[41] the scaling parameter is the projectile velocity. For damped reactions, where a range of impact parameters can be scanned, rather scarce data seem to suggest a correlation between the multiplicity of nonequilibrium neutrons and the radial approach velocity, or the radial kinetic energy per nucleon at touching. This type of systematics is illustrated in Fig. 3, where the estimated multiplicity $<m_{pre}>$ of nonequilibrium neutrons in coincidence with PLFs is plotted[31] versus radial nucleus-nucleus energy E_{rad} per nucleon at touching, for three different reactions. Over a limited range of bombarding energies, the data appear to define a universal correlation of the form

$$<m_{pre}> \approx 0.217\ (E_{rad} - 2\ \text{MeV})/\mu \qquad (1)$$

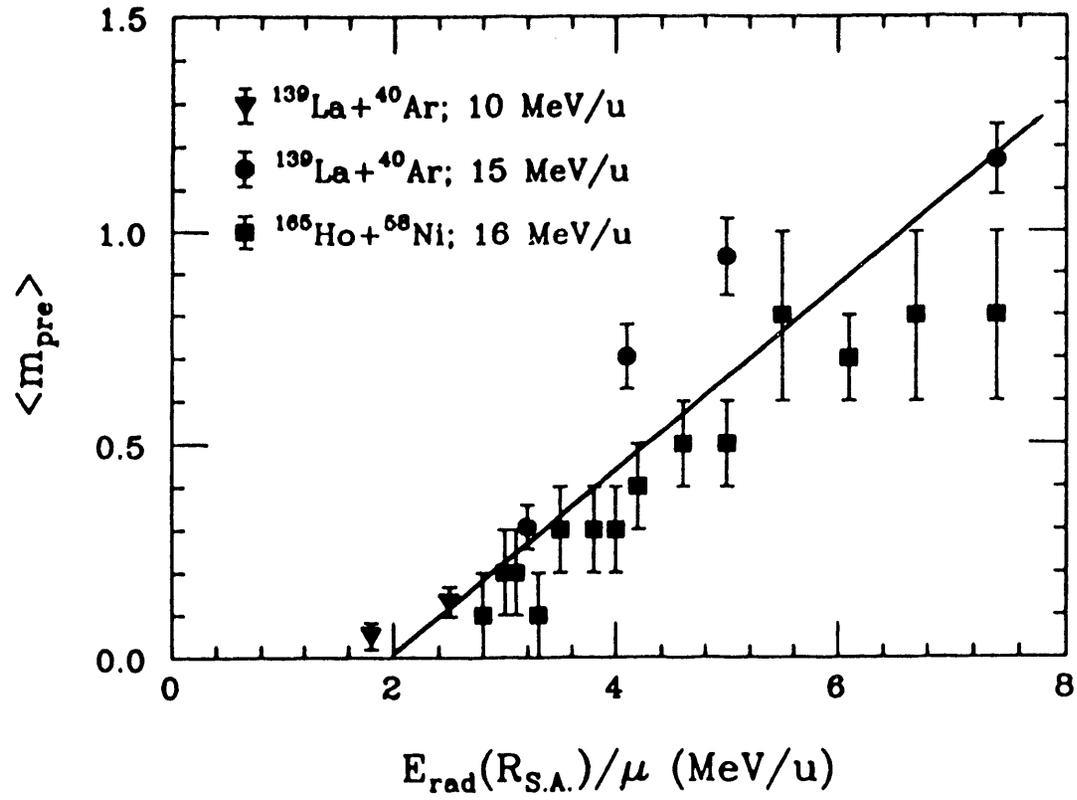
1.5
1.0
0.5
0.0
0
2
4
6
8
^{139}La+^{40}Ar; 10 MeV/u
^{139}La+^{40}Ar; 15 MeV/u
^{165}Ho+^{58}Ni; 16 MeV/u
$\langle m_{pre} \rangle$
$E_{rad}(R_{S.A.})/\mu$ (MeV/u)

Figure 3

where μ is the reduced mass in the entrance channel. The energy spectra of these particles are of a Maxwell-Boltzmann type, decreasing exponentially in intensity toward high energies, consistent with a decay constant of

$$<T_{pre}> \approx 1.7 \text{ MeV} + 0.44 (E-V_c)/\mu \quad (2)$$

known[41] from heavy-ion fusion reactions.

Here, V_c is the Coulomb energy at touching ($r = R_{SA}$) in the entrance channel. More recently, a similar trend with impact parameter has been observed[43] for the multiplicities of nonequilibrium light charged particles emitted in medium-energy heavy-ion reactions.

Not much is known about the systematics of nonequilibrium particle emission at energies above 10-15 MeV/u. However, if the above trends continue in a linear fashion, nonequilibrium particle emission would present a very effective mechanism of instantaneous cooling of nuclear systems at bombarding energies in the Fermi energy domain. The process could easily account for the apparent limitations in energy deposition reported[44,45] energetic Th + Ar collisions. The effect, could prevent attainment of nuclear temperatures required for the onset of the new reaction mechanisms of multifragmentation or vaporization discussed previously.

Experimental data on nonequilibrium or jet particle emission are not reproduced consistently by preequilibrium models[46-48] that were originally designed for reactions induced by light projectiles but adapted to some extent to heavy-ion collisions. Similar insufficiencies in the reproduction of experimental data have been reported[31,49] for Fermi jet models,[50-52] that have been developed particularly for applications in heavy-ion reactions.

2.2. Associated Light Particles as Heat Sensors

For heavy-ion reactions at bombarding energies of a few tens of MeV per nucleon, nonequilibrium particle multiplicities are small[31,43] compared to the numbers of equilibrium neutrons and light particles evaporated sequentially from the hot nuclear system. The

multiplicities and angle-energy patterns of these latter particles can be employed to deduce the intrinsic excitation energy of the system with which this "vapor" of particles is in statistical equilibrium. The particle emission patterns can be determined by detector arrays such as depicted in Fig. 4, used to measure neutrons in coincidence with PLFs from the reaction $^{197}Au + ^{208}Pb$ at 29 MeV/u. In this setup, 21 neutron detectors were placed in plane with solid-state detector telescopes measuring charged products, while two detectors were mounted in out-of-plane positions.

As will be illustrated in Section 3, this number of detectors is sufficient to disentangle the contributions of neutrons emitted from various different sources. The individual contributions can be inferred approximately from fits to the experimental double-differential multiplicity distributions with superpositions of theoretical distributions of the form[53]

$$\frac{d^2m}{dEd\Omega} = \frac{m}{2(\pi T)^{3/2}} \sqrt{E}\ \exp\{-(E-2\sqrt{\epsilon E}\cos\theta + \epsilon)/T\} \qquad (3)$$

The equivalent distribution for charged particles depends on the barrier height V_B for emission, modifying the preeexponential factor. In Eq. (3), E stands for the laboratory neutron energy, m for the integrated multiplicity, ϵ is the laboratory energy per nucleon of the emitter, and θ denotes the neutron emission angle relative to the direction of flight of the emitter. For the emission of a single neutron, T represents the temperature of the daughter nucleus. For a cascade of several neutrons emitted in succession, the parameter T is an effective quantity.[54] In general, detailed simulation calculations are required to interpret the experimental distributions. These simulations have to include the detector geometry and efficiency, in particular for coincidence measurements that impose kinematical constraints on the particles to be measured.

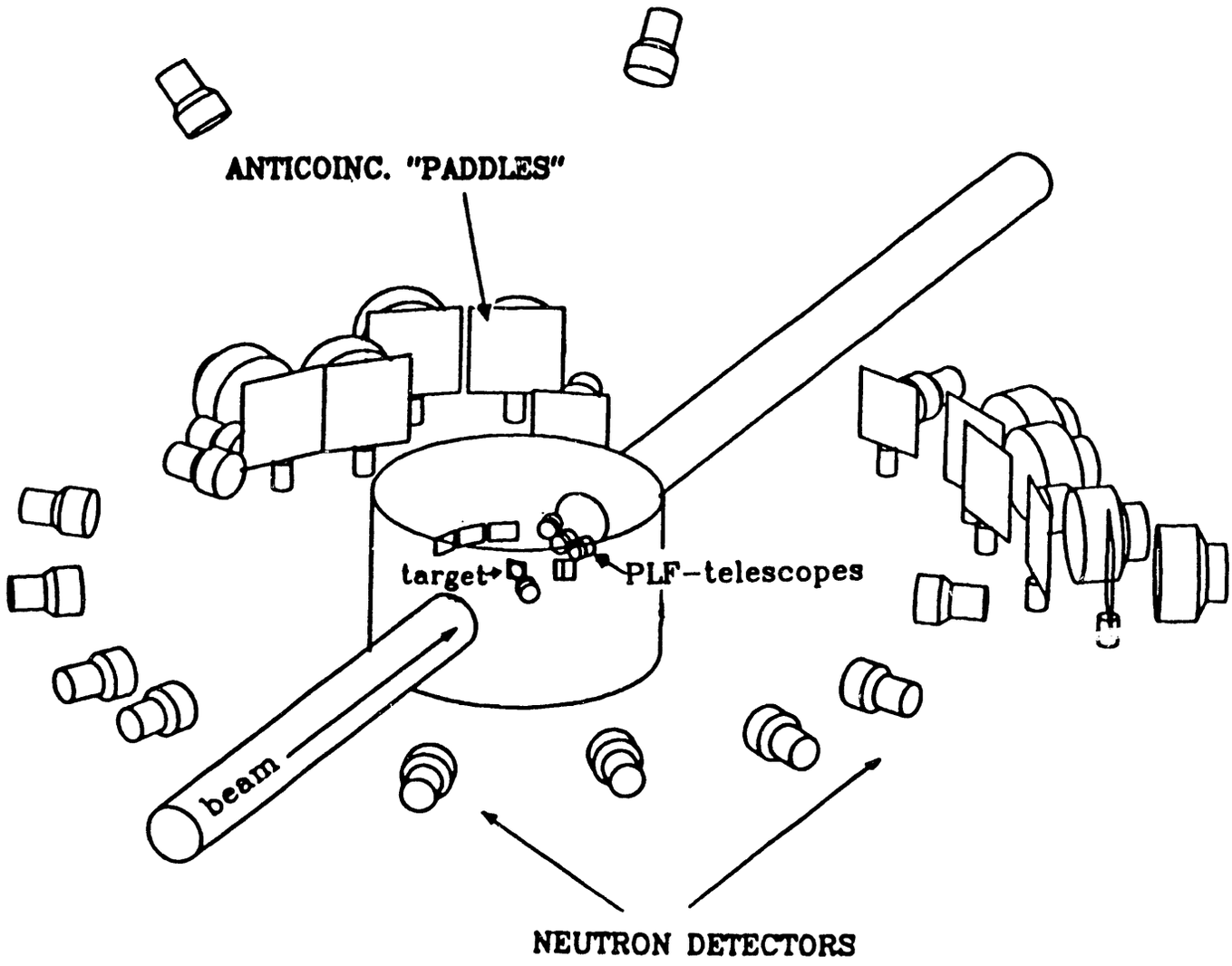
ANTICOINC. "PADDLES"
target
PLF-telescopes
beam
NEUTRON DETECTORS

Figure 4

However, a good estimate of the excitation energy contained in a nuclear system can be obtained already from the multiplicity of the emitted particles. The average excitation energy

$$-\overline{\delta E^*} = \overline{(-\Delta E^*/\text{particle})} \approx \overline{B} + (\overline{V_B} + \overline{E}) \approx \overline{B} + \overline{V_B} + 1.5T \qquad (4)$$

Here, $\overline{B}$ is the average particle binding energy ($\overline{B} \approx$ 8-10MeV). For the bombarding energies of interest here, the spectral slope parameter T is of the order of a few MeV at most. Since $T \leq (\overline{B} + \overline{V_B})$, this parameter can be estimated from systematics reasonably accurately, for the purpose of calculating $\overline{\delta E^*}$.

Both the distribution of multiplicities of neutrons and that of light charged particle emitted from a nucleus are expected to provide independent measures of the nuclear excitation energy distribution, but with different intrinsic resolutions. Since $V_B = 0$ for neutrons, the highest resolution is, in principle, attainable with neutrons. However, the relation between excitation energy E^* and particle multiplicity m is in general nonlinear. This is due to the fact that the cumulative binding energy B(m) for m particles increases quadratically with m, while the average spectral slope parameter T increases with the square-root of the initial excitation energy.

This nonlinearity is illustrated in Fig. 5 for neutrons emitted from excited ^{197}Au nuclei. A simplified neutron evaporation calculation[55] has been performed, for excitation probability distributions that are constant from $E^* = 0$ to the maximum excitation energies E^* noted at the various curves in Fig. 5. From such excitation energy distributions, one obtains multiplicity distributions increasing linearly with multiplicity since the multiplicity bin width is determined by dB/dm. For the same reason, the upper edge of the multiplicity distribution, as well as the most probable multiplicity do not move to higher multiplicities in proportion to the maximum excitation energy of the emitting nucleus.

As a result, one expects and, in fact, observes particle multiplicity distributions that reflect the shape of the excitation energy distributions to a certain extent but exhibit a peak at high multiplicities, partially due to the above nonlinearity effect. For example, the

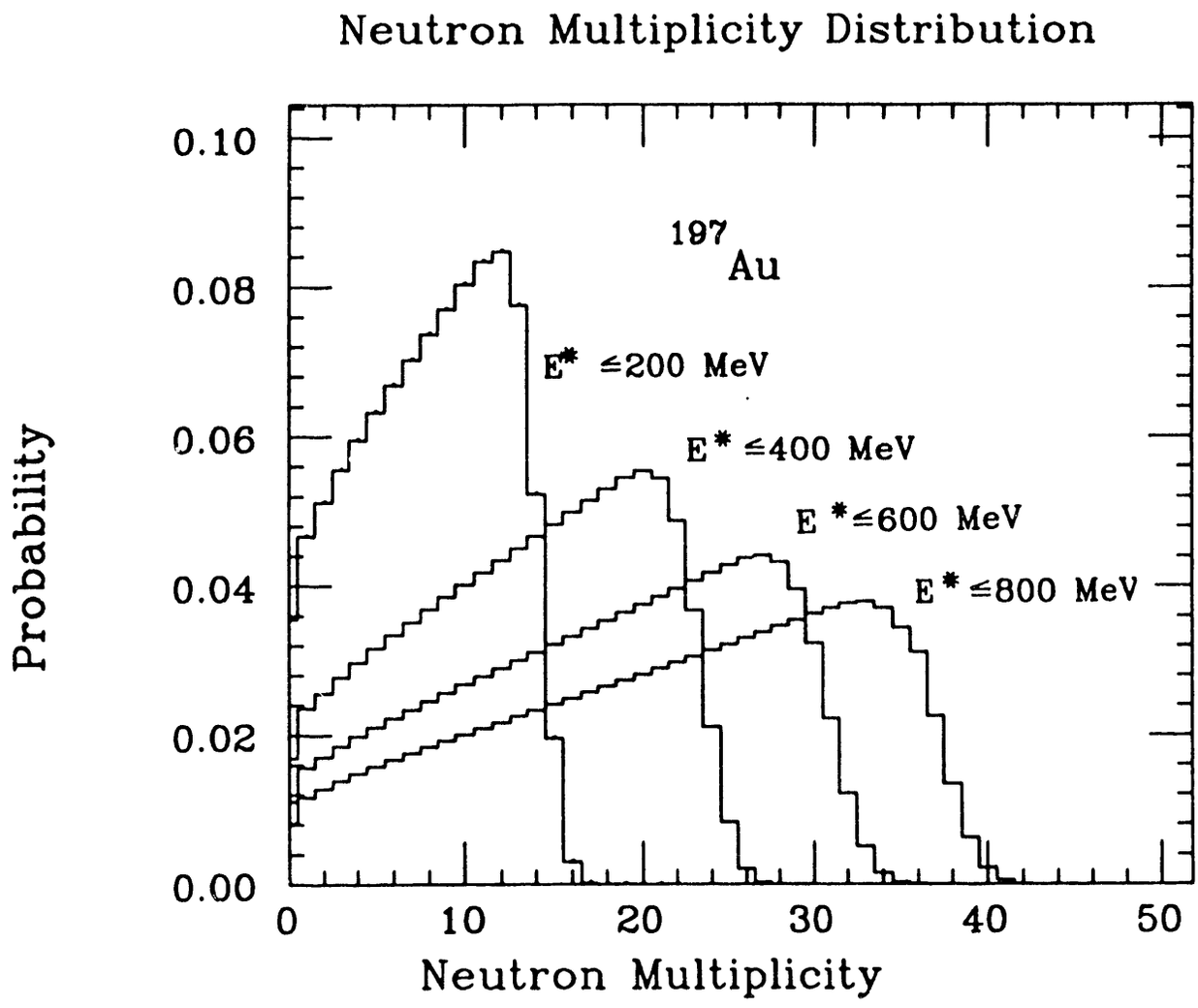
Neutron Multiplicity Distribution
Probability
0.10
0.08
0.06
0.04
0.02
0.00
197 Au
E* ≤200 MeV
E* ≤400 MeV
E* ≤600 MeV
E* ≤800 MeV
0
10
20
30
40
50
Neutron Multiplicity

Figure 5

multiplicity distributions resulting from the damped energy loss spectra of Fig. 2 look similar to the latter distributions but feature "central collision peaks" that are relatively much narrower than the broad bumps visible in the energy loss spectra of Fig. 2. A fast emission of nonequilibrium particles with the broad energy spectra characterized by multiplicities and slope parameters given by Eqs. (1) and (2), respectively, will both shift the average of the high-multiplicity peak to lower values and broaden it.

With the above qualifications, the multiplicities of particles evaporated from a hot nucleus, in particular the neutron multiplicity, can be employed to deduce the (thermal) excitation energy. In the present work on the $^{209}Bi + ^{136}Xe$ reaction, carried out at the MSU K1200 cyclotron, the method has been used both for neutrons and charged particles. In order to obtain a good measure of the total neutron multiplicity in a collision, a 4π neutron multiplicity meter[56-59] (NMM) was used, i.e., a scintillation detector containing Gd-doped liquid scintillator. The Rochester 900-ℓ NMM utilized in the MSU experiment is pictured at the top of Fig. 6, while the $^{197}Au + ^{208}Pb$ measurement made use of the large ($\sim 3m^3$) NMM ORION[30,60] installed at the GANIL facility. The $^{197}Au + ^{208}Pb$ reaction, has been investigated with measurements[61-63] of the total neutron multiplicity and a neutron time-of-flight experiment,[49] both performed at GANIL. All of these experiments represent exclusive measurements of neutrons in coincidence with charged reaction products. This is the first time that neutrons and charged particles emitted in a heavy-ion reaction have been measured in coincidence with essentially 4π coverage for all particles.

In the former experiment, the Dwarf Ball/Wall multi-detector array[64,65] was inserted into the internal chamber of the Rochester NMM to provide full coverage for light charged particles.[66] A segment of the Wall was replaced by several triple solid-state telescopes for the detection of massive charged products.

The principle of operation[56-59] of both of the above NMMs is the same. Neutrons emitted in a nuclear reaction taking place in the internal scattering chamber of the NMM enter the liquid-scintillator volume, where they are rapidly slowed down by elastic

Neutron Multiplicity Meter

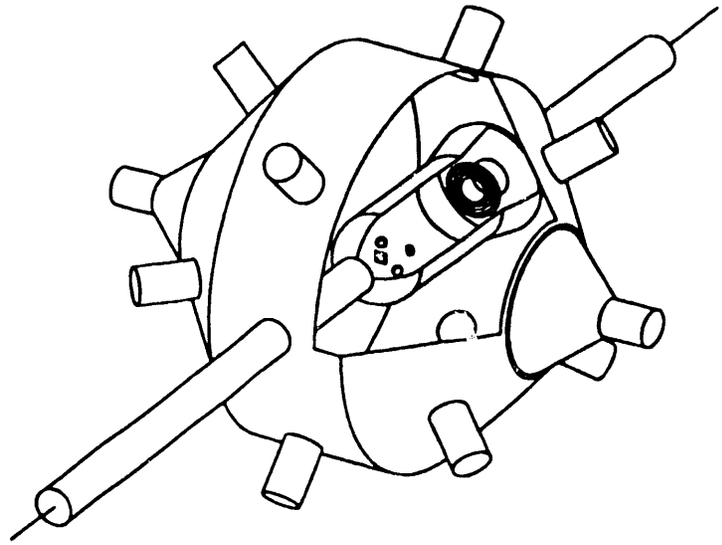

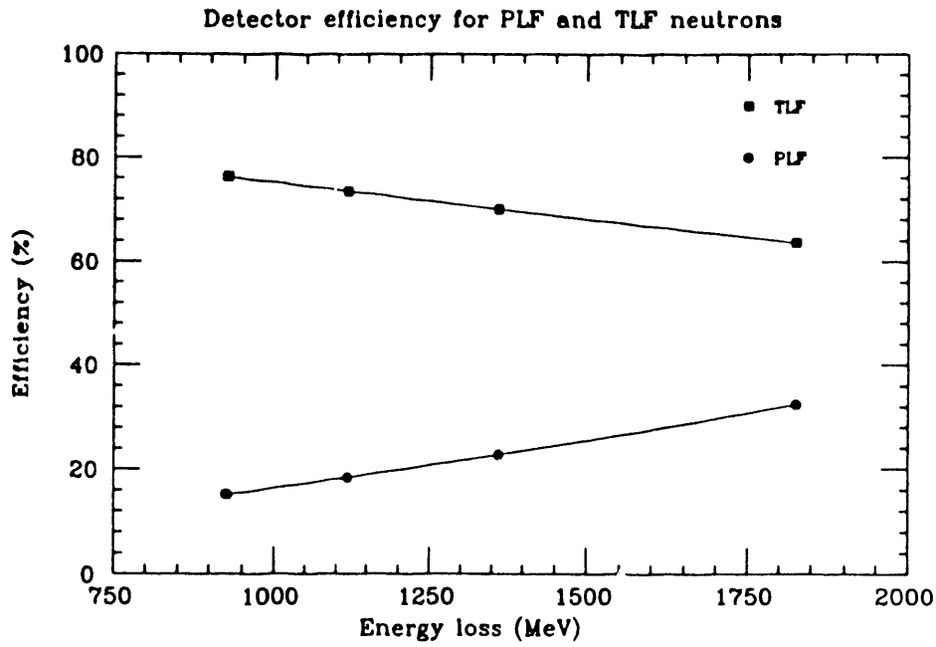

Figure 6

collisions with the protons of the organic scintillator material. Thermalized neutrons then diffuse through a region within the scintillator tank, until they are captured by Gd nuclei. The capture γ-rays then produce scintillation light detected by photomultipliers viewing the scintillator. Due to the slow diffusion of the neutrons, the capture times are statistically distributed over a time interval of tens of micro-seconds, allowing one to deduce the neutron multiplicity simply by counting the number of capture events.

High neutron detection efficiencies are needed to measure the large neutron multiplicities occurring in medium-energy heavy-ion collisions with sufficient accuracy. While efficiencies in excess of $\varepsilon = 0.9$ can be reached for ^{252}Cf-fission neutrons, these numbers are significantly smaller for the neutrons emitted from fast-moving, hot fragments produced in heavy-ion collisions, due to the smaller scattering cross sections at the higher neutron energies.

The bottom part of Fig. 6 displays the efficiencies expected[67] for neutrons emitted sequentially from the PLFs and TLFs produced in binary ^{209}Bi + ^{136}Xe collisions, at 28 MeV/u. Here, the efficiencies are plotted versus the kinetic-energy loss suffered in a collision, as calculated with a modified version[59] of the efficiency code[57] DENIS. Due to the large differences in PLF and TLF velocities, the efficiencies for neutrons emitted from the respective fragments are rather different. This is, in principle, a desirable effect, allowing one to distinguish between the various neutron components. With increasing energy loss, the disparity in detection efficiency decreases, since the momentum transfer from PLF to TLF increases. The selectivity of the Rochester NMM to neutrons from the TLF is assisted by the particular design of the internal NMM scattering chamber, featuring an "escape cone" permitting neutrons emitted into forward angles ($\Delta\theta = \pm 22°$) from the fast-moving PLF to escape the NMM without interaction with the scintillator. A discrimination between the different neutron groups is facilitated[60] with NMMs that are segmented, like the GANIL device ORION. Such a segmentation provides the opportunity

to measure a coarse angular distribution of the individual neutrons, since the capture sites are found to be located in the vicinity of the initial neutron trajectory.

In addition to the delayed part of the overall response signal of an NMM, associated with neutron capture events, there is a well-separated prompt part of the light output signal. This prompt signal contains information on the total energy of the nuclear system carried away by neutrons and, to a lesser extent, by the prompt reaction-γ-rays. An example is given in Fig. 7, where the yield measured in the reaction ^{209}Bi + ^{136}Xe at 28.2 MeV/u is plotted on logarithmic scale versus neutron multiplicity and prompt light output, in an isometric representation (Fig. 7, top) or in form of a contour diagram (Fig. 7, bottom). For this particular plot, a prompt NMM signal was recorded only in coincidence with a particular trigger telescope, while the multiplicity measurement was triggered also by other charged-particle detectors. Hence, on the left in Fig. 7, there appears an intense multiplicity ridge not associated with a prompt signal. The main interest in this figure is, however, the correlation observed between the prompt pulse-height and the neutron multiplicity. The width of the correlation pictured in Fig. 7 is partially due to the finite widths of neutron and fragment energy spectra and partially an effect of NMM resolution. It has been suggested earlier[69] to employ the prompt response of a plastic-scintillator device to a multi-neutron event in deducing the neutron multiplicity.

3. DISSIPATIVE REACTION FEATURES OF VERY HEAVY SYSTEMS

3.1. Dissipation, Evaporation, and Disassembly in the Reaction ^{197}Au + ^{208}Pb at 29 MeV/u

In this section, results are reported on two different experiments on the very heavy, symmetric system ^{197}Au + ^{208}Pb, using the 29-MeV/u ^{208}Pb beam of the GANIL accelerator complex. The goal of an exclusive neutron time-of-flight experiment,[49] performed with the setup illustrated in Fig. 4, was to study neutron emission patterns as functions of kinetic energy and atomic number of coincident massive reaction products. Of

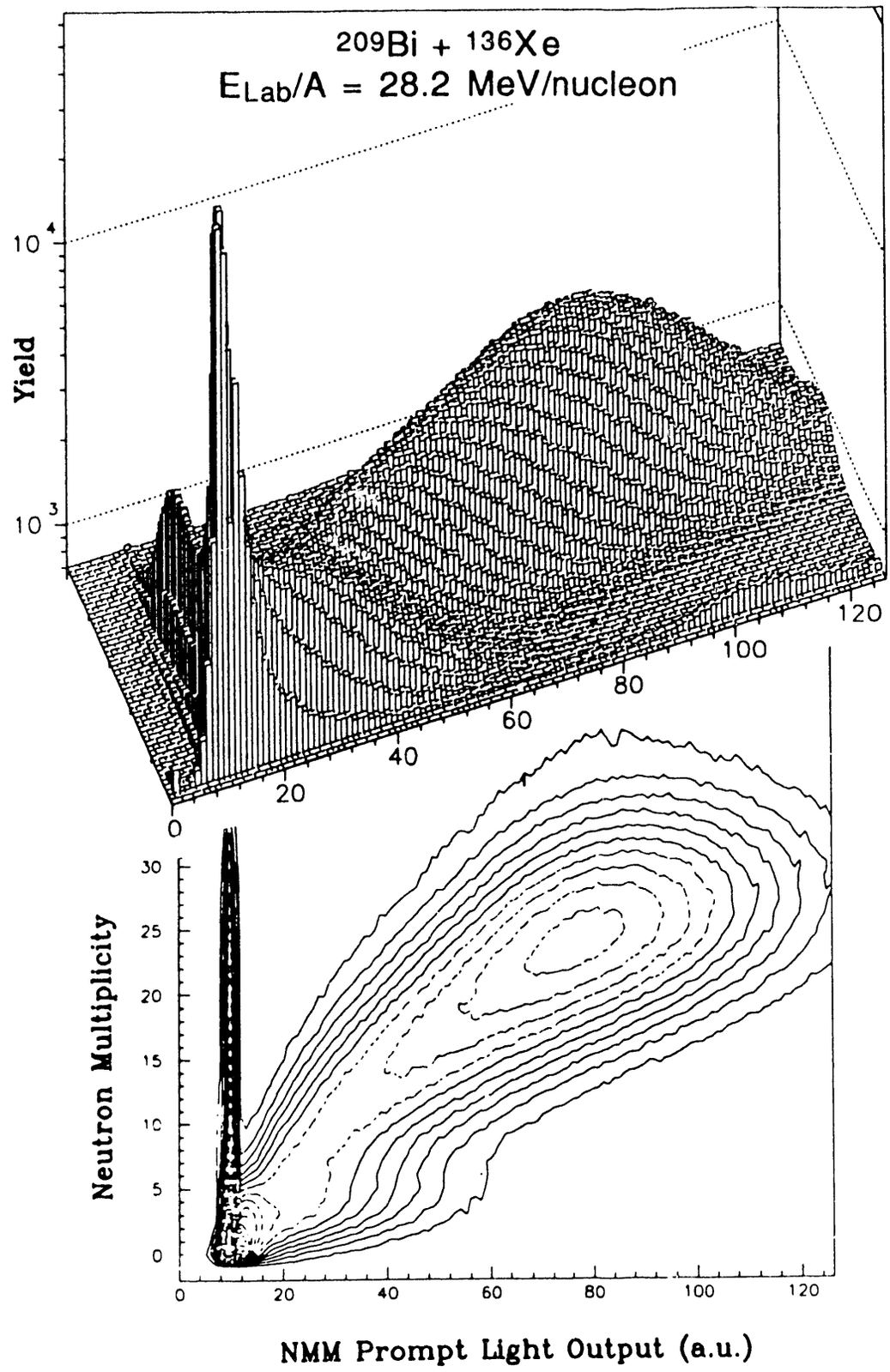
209Bi + 136Xe
ELab/A = 28.2 MeV/nucleon
Yield
10^4
10^3
0
20
40
60
80
100
120
Neutron Multiplicity
30
25
20
15
10
5
0
NMM Prompt Light Output (a.u.)

Figure 7

particular interest was to explore to what extent the neutron flow, observed in coincidence with PLFs could be understood in terms of emission from equilibrated fragments produced in binary dissipative collisions. Another objective of this experiment has been to determine the relative importance of nonequilibrium emission of jet-like neutrons. The emphasis of this experiment was placed on peripheral reactions, in order to make contact with the binary collision phenomena at lower bombarding energies.

A second experiment[61-63] focused instead on the efficiency of the neutron multiplicity as a reaction or impact-parameter filter. This experiment utilized the NMM ORION at GANIL, operated both in singles and in coincidence with three-member telescopes detecting charged products from the $^{197}Au + ^{208}Pb$ reaction.

As a sample of the results obtained in the former, time of flight experiment, Fig. 8 shows the distribution of charged fragments ($Z \geq 10$) versus Z and E as detected at $\theta = -6.5^{\circ}$, i.e., near the grazing angle ($\theta_g \approx 6^{\circ}$) for this reaction. The logarithmic contour lines are for yields that differ by factors of ten. Due to the finite detection threshold, most fragments detected at this angle are associated with the projectile, i.e., represent PLFs or their evaporation products. Lead-like fragments originating from partially damped reaction processes are the dominant fragment group and form an intense peak at high energies. A continuous cross section ridge extends from the quasielastic peak at $Z \approx 82$ and $E \approx 5.8$ GeV down into the region of PLF-fission fragments. Fission of the excited, fast-moving PLF leads to two groups of fragments, one of which is responsible for the excursion of cross section at $Z \approx 40$ and $E \approx 4.5$ GeV. A group of intermediate-mass fragments (IMF) is observed at $Z \leq 20$ and $E \leq 0.5$ GeV. The approximately constant slope of the cross section ridge in the Z vs. E diagram could be taken as as indication of the memory of the projectile velocity retained in the PLF-distribution resulting from a fragmentation-type process (cf. Fig. 1). On the other hand, a similar correlation results from evaporative decay of the hot primary fragments produced in a damped collision. Detailed simulation calculations discussed further below are required to distinguish between these two

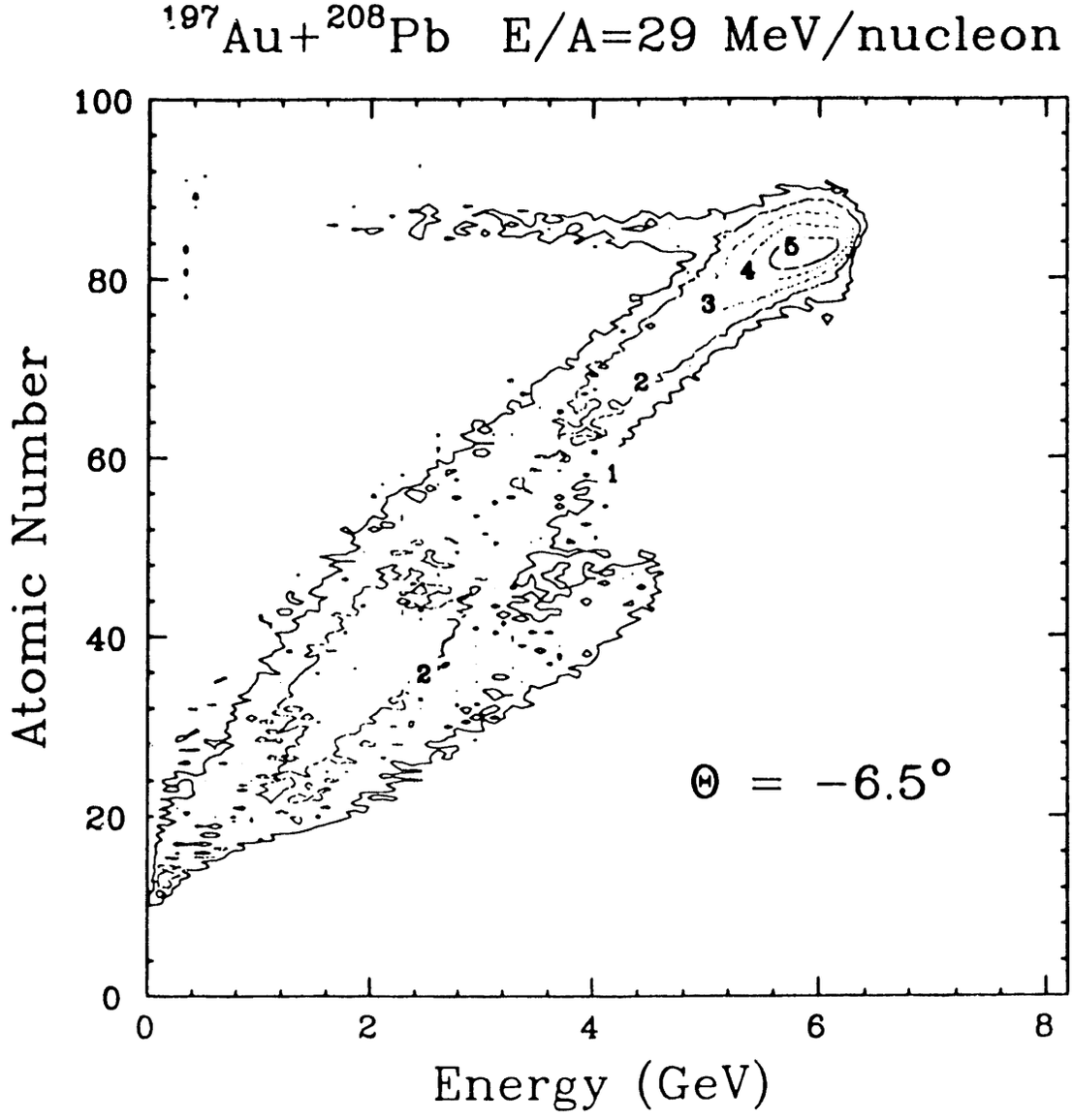
^{197}Au+^{208}Pb E/A=29 MeV/nucleon
Atomic Number
Energy (GeV)
Θ = −6.5°
0
20
40
60
80
100
0
2
4
6
8
1
2
3
4
5
2

Figure 8

alternatives. For the purpose of a first cursory analysis, two different regions are defined in the Z-E-plane, which in a binary reaction scenario correspond to different ranges of energy loss. The region of $Z \geq 80$ and $E \geq 5$ GeV is tentatively attributed to partially damped collisions, while that for $55 \leq Z \leq 70$ is identified with strongly damped collisions. The spurious ridge at high Z-values is due to slit scattering.

Fig. 9 shows Galilei-invariant velocity spectra of neutrons measured at 8 selected angles in coincidence with fragments from partially damped collisions, as defined above. At backward angles, the distributions show a monotonic decay towards high velocities, as is characteristic for neutron evaporation from a relatively slow, equilibrated source such as represented by TLFs. At forward angles, the neutron spectra exhibit additional structure. Here, a high-velocity component is observed to be centered at $v_n \approx 6.5$ cm/ns, i.e., somewhat less than the beam velocity of $v_b = 7.5$ cm/ns. This latter component is characteristic of emission from fast-moving PLFs.

Simple calculations were performed modeling sequential evaporation of neutrons from PLFs and from their TLF reaction partners, using moving-source parameterizations of the type represented by Eq. (3) for PLF and TLF. For this partially damped group of events, an average energy loss of $\approx$ 140 MeV was estimated from binary kinematics. A slope parameter of T = 1.8 MeV was adopted for both PLF and TLF, as is consistent with this energy loss. Although the experimental yield at $\theta_{lab} = -15°$ is somewhat overestimated, the above parameterization (dashed-dotted curves) provides a satisfactory representation of the data. However, this two-source model does not provide an adequate explanation of the yield at high velocities for $\theta_{Lab} = -62°$ and 37.8°. The excess yield seen at these angles is attributed to an additional nonequilibrium emission process, such as observed[31] already at lower bombarding energies. The emission pattern of the corresponding neutrons is modeled here (dotted curves) with a Fermi-jet process[52] for a single effective angular momentum of $\ell_{eff} = 1.5k\hbar$. Combined, these two models (solid curves) provide a reasonable explanation of the observed spectra. Compared to the spectra

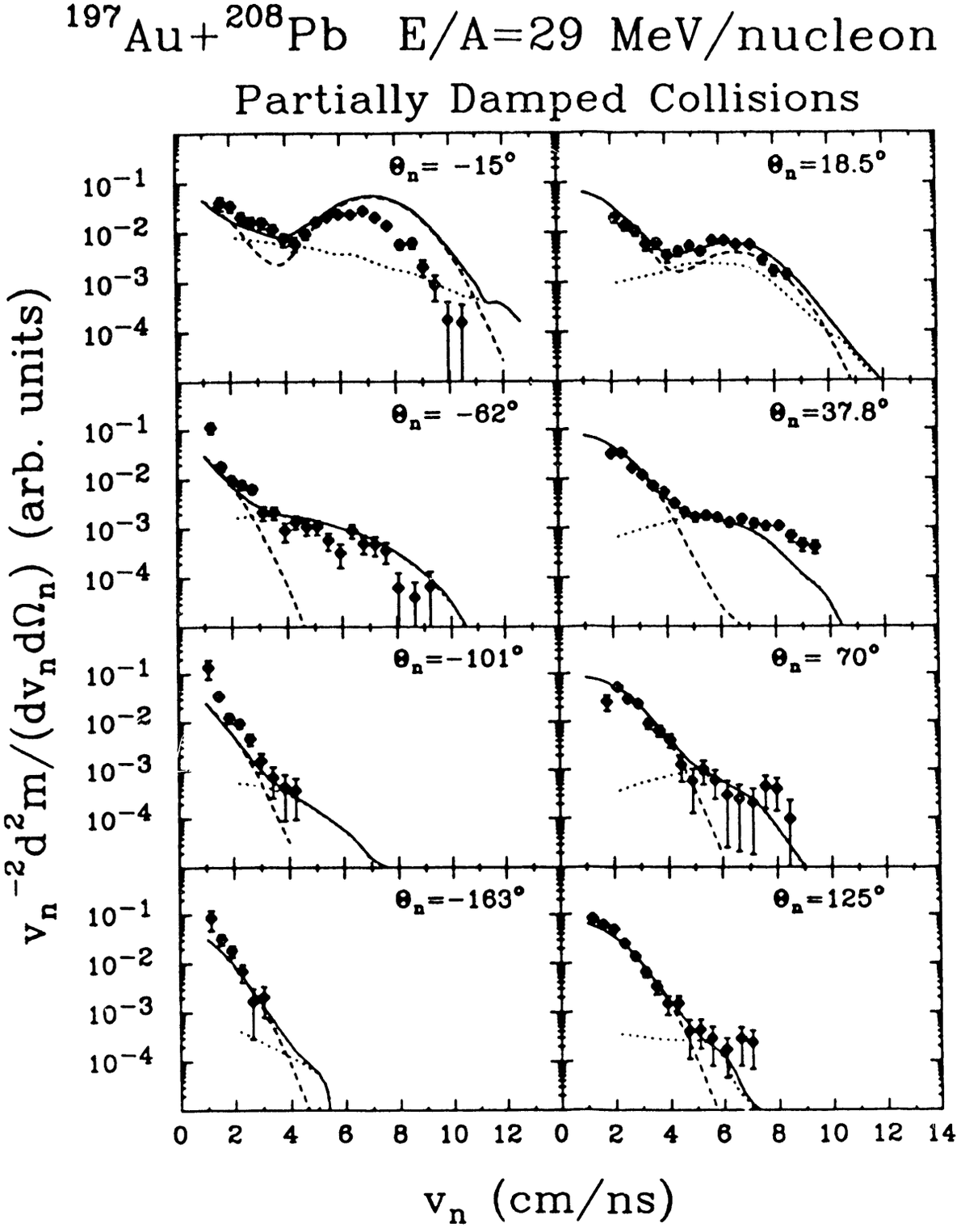
197Au+208Pb E/A=29 MeV/nucleon
Partially Damped Collisions
θn= -15°
θn=18.5°
θn= -62°
θn=37.8°
θn=-101°
θn= 70°
θn=-163°
θn=125°
10-1
10-2
10-3
10-4
0 2 4 6 8 10 12 0 2 4 6 8 10 12 14
vn -2d2m/(dvndΩn) (arb. units)
vn (cm/ns)

Figure 9

of Fig. 9, the neutron spectra associated with strongly damped events shown in Fig. 10 appear relatively structureless, although two components are still visible at forward angles. Due to the large multiplicities of neutrons evaporated from the PLFs and the high neutron laboratory energies, the relatively small jet component predicted (dotted curves) by the same calculation as above, but for $\ell_{eff} = 1.2k\hbar$, would be completely masked. Hence, a satisfactory description of the spectra is already obtained assuming two equilibrated fragments, PLF and TLF, as the only sources of neutrons. The fits shown in Fig. 10 were obtained assuming T = 4.9 MeV and an average estimated energy loss of $E_{Loss} \approx$ 1.3 GeV.

From the neutron spectra of Figs. 9 and 10, representing only a fraction of the available data for this system, it can be concluded that sequential emission from accelerated fragments is dominant for relatively peripheral or intermediate collisions. Such a behavior is expected in a binary reaction scenario. For example, calculations with the code CLAT [68] based on the one-body exchange model,[4-5] reproduced in Fig. 11 for $\ell = 1.45k\hbar$. This figure depicts the evolution of the dissipated energy E_{diss}, the relative velocity v_{rel}, the dinuclear temperature τ and of an estimated particle evaporation time t_n with time. The calculation suggests that the interaction does not generate heat fast enough to produce significant particle evaporation before the system reseparates and accelerates. Although this consistency of the data with a binary damped reaction scenario does not prove the dominance of this mechanism at 29 MeV/u, the observations are not easily understood in terms of a participant-spectator picture, where both projectile and target spectators are left in a relatively cold state.

Knowledge of the emission patterns of neutrons in a reaction assists in the interpretation of neutron multiplicity distributions measured with NMMs in experiments not utilizing the available information on the neutron energy and angular distribution. The total neutron multiplicity distribution obtained[61] for the reaction $^{197}Au + ^{208}Pb$ in singles, using the ORION NMM, is depicted in Fig. 12. It has not yet been corrected for the finite

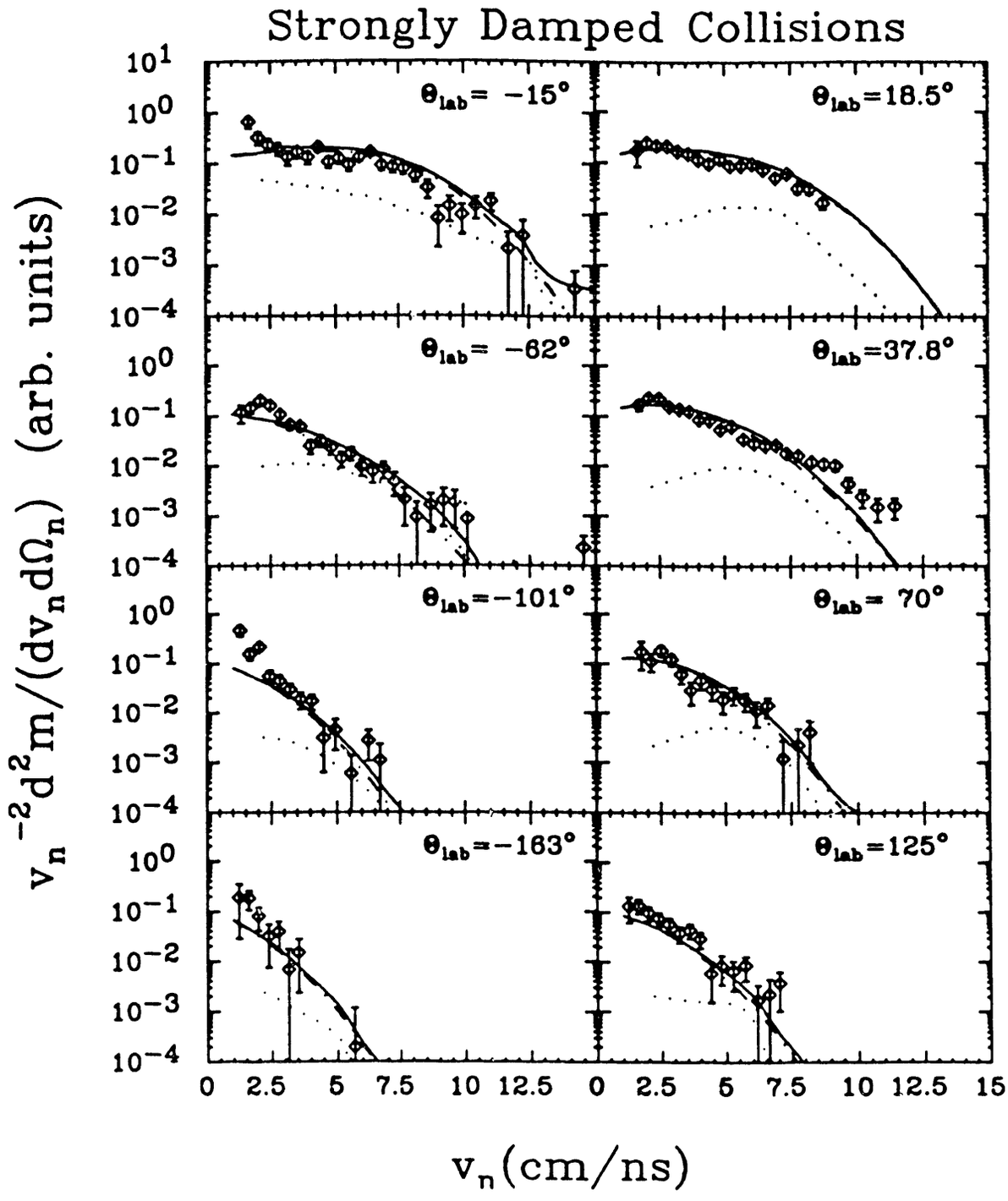
Strongly Damped Collisions
θ_{lab}= −15°
θ_{lab}=18.5°
θ_{lab}= −62°
θ_{lab}=37.8°
θ_{lab}=−101°
θ_{lab}= 70°
θ_{lab}=−163°
θ_{lab}=125°
$v_n^{-2} d^2m/(dv_n d\Omega_n)$ (arb. units)
v_n(cm/ns)

Figure 10

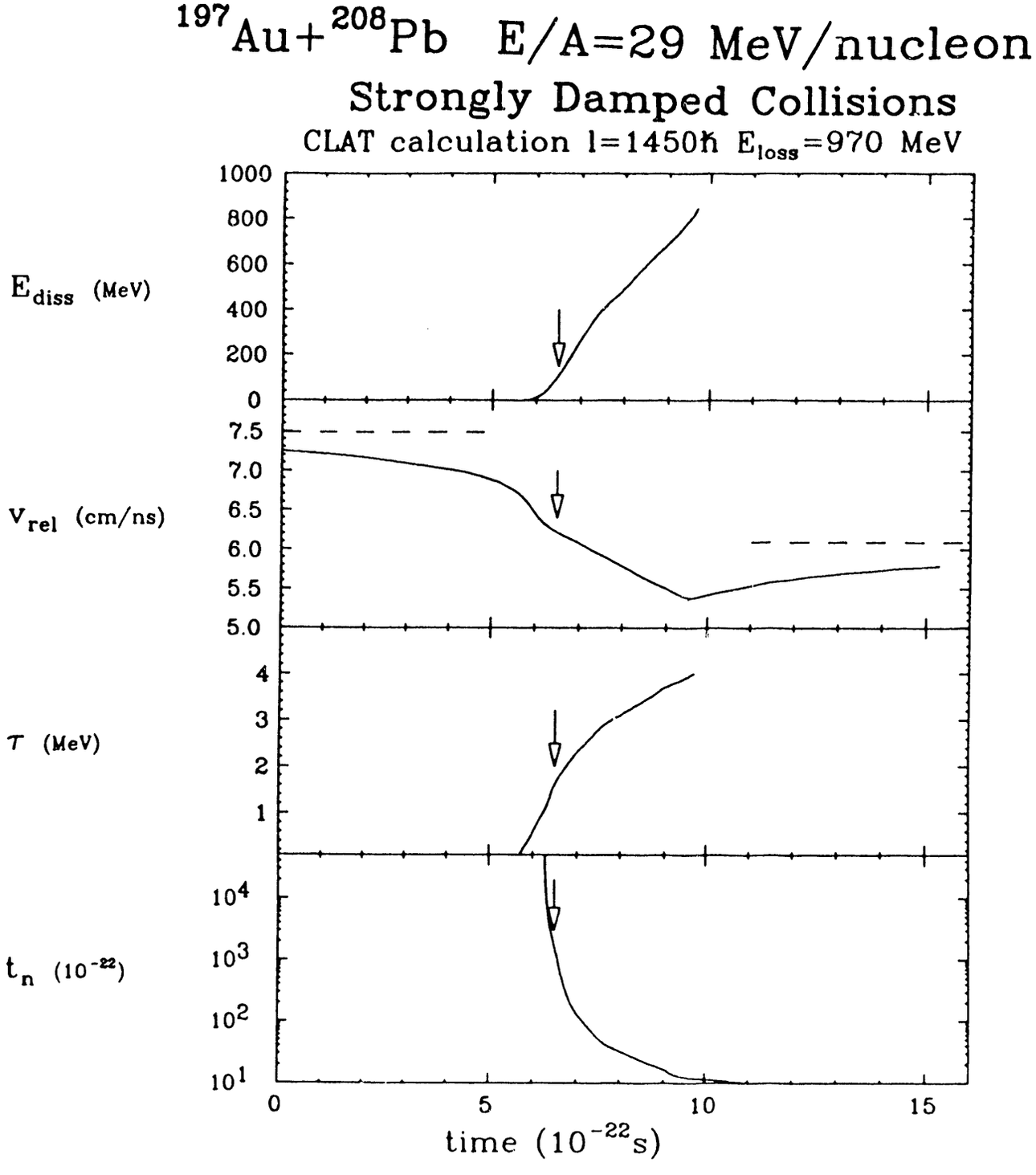
197Au+208Pb E/A=29 MeV/nucleon
Strongly Damped Collisions
CLAT calculation l=1450ħ E_loss=970 MeV
E_diss (MeV)
V_rel (cm/ns)
T (MeV)
t_n (10^-22)
time (10^-22 s)

Figure 11

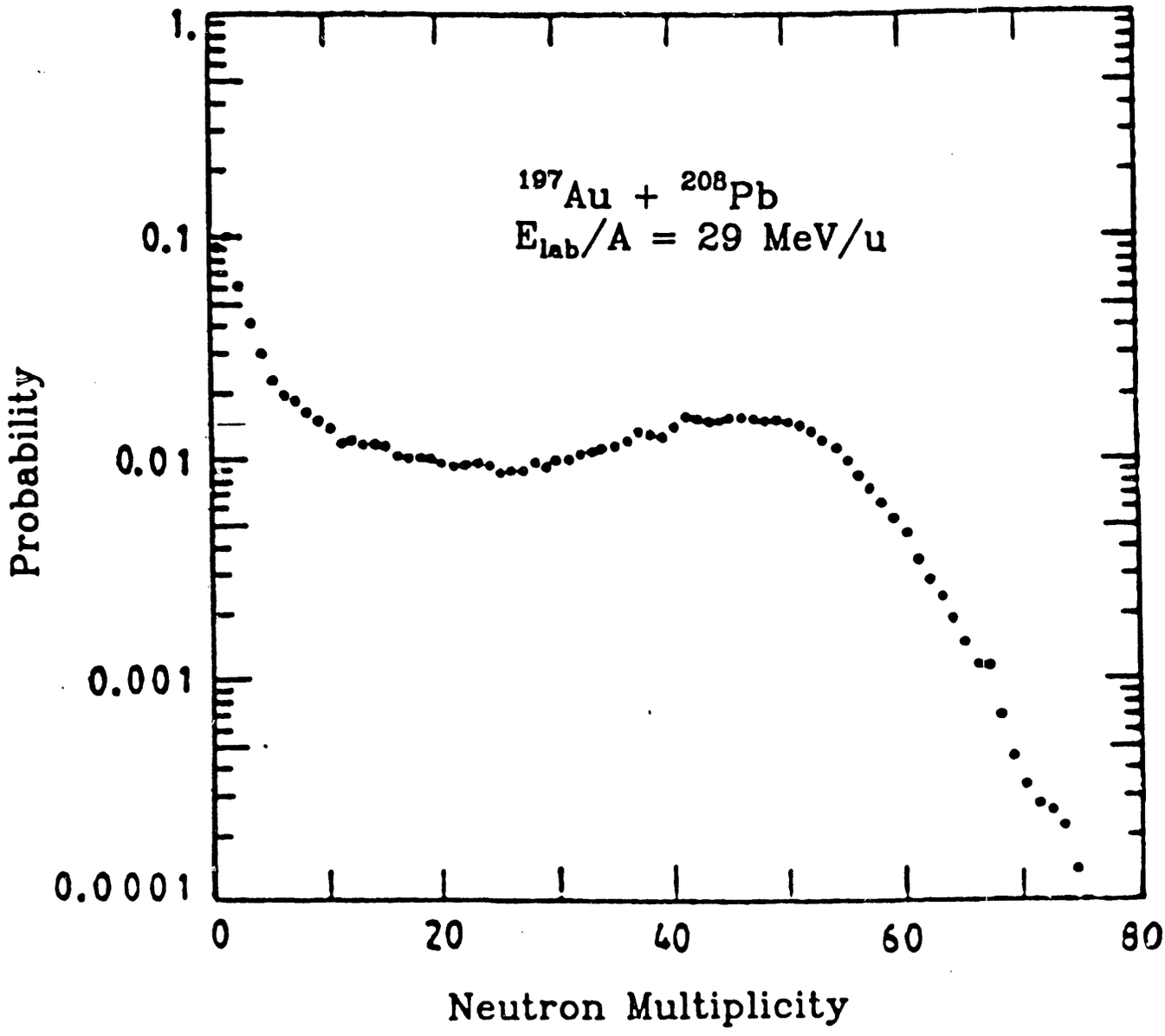
1.
0.1
0.01
0.001
0.0001
Probability
$^{197}Au + ^{208}Pb$
$E_{lab}/A = 29$ MeV/u
0
20
40
60
80
Neutron Multiplicity

Figure 12

efficiency of the NMM. However, the measured distribution reflects a shape expected from a binary collision scenario, as discussed in the contexts of Figs. 2 and 5. A shoulder at low multiplicities is associated with peripheral reactions, the object of the neutron time-of-flight study discussed above. This feature merges with a broad multiplicity bump attributed to the more central collisions. It has been argued in Section 2 (cf. Fig. 5) that such a bump arises naturally even for flat excitation energy distributions. The most probable neutron multiplicity, measured to equal m = 50, corresponds to approximately 78 neutrons, when corrected for NMM efficiency. This number represents about one-third of all the neutrons in the system.

Since the above neutron time-of-flight study suggests strongly that low-energy reaction patterns extend to bombarding energies near the Fermi energy domain, one would expect the measured neutron multiplicity to reflect the total excitation energy in PLF and TLF and, hence, to provide a measure of the collision impact parameter. The detection efficiencies of the NMM are, similar to the dependencies illustrated in Fig. 6, much higher for neutrons from slow-moving emitters than for those emitted either from fast-moving sources such as the PLF, a hot participant zone (cf. Fig. 1), or a "fireball". Therefore, strong and very characteristic dependencies of the reaction patterns on the measured (and possible strongly biased) neutron multiplicity are expected to manifest themselves, if a binary, damped reaction mechanism prevails. Such features would not be expected from a predominant spectator-participant reaction mechanism.

The sequence [61] of charged-product distributions from the $^{197}Au + ^{208}Pb$ reaction displayed in Fig. 13 for successive bins in observed neutron multiplicity n is quite suggestive of a prevailing primary reaction mechanism reminiscent of the low-energy damped reaction scenario, at least for low and intermediate multiplicities. The distributions, shown in Fig. 13 on logarithmic intensity scale except for the one on the top left, are plotted versus energy (x) and energy loss (y) in the first two elements of a Si detector hodoscope spanning an angular range from 6.1° to 20°. For the lowest

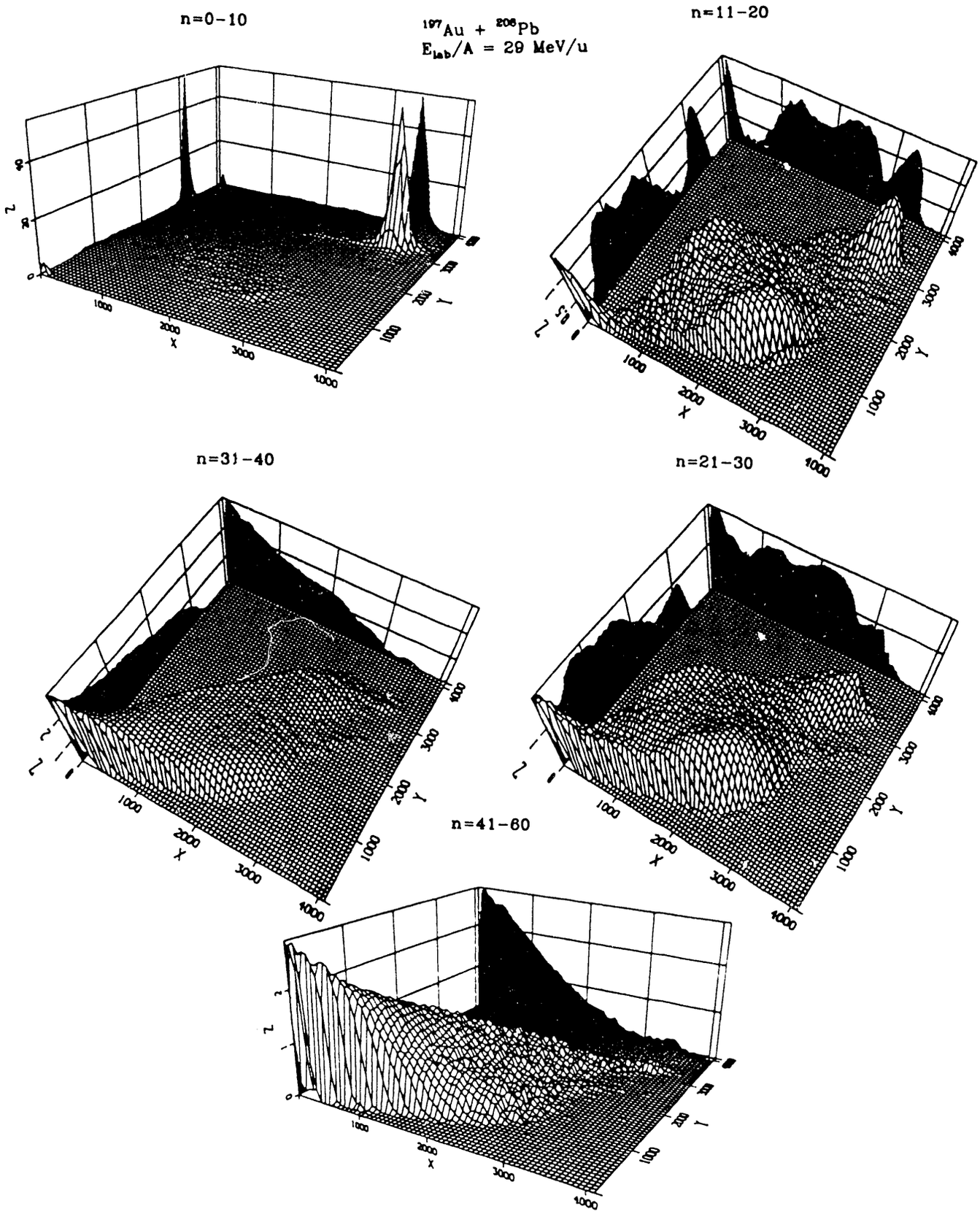

Figure 13

multiplicities, the distribution is dominated by a peak of elastic and quasi-elastic events, developing into a broad bump of damped PLF fission fragments. In addition, a component of PLF fragments is visible for intermediate multiplicities, as has already been discussed in the context of Fig. 8.

It is observed from Fig. 13, that the relative yield of massive PLF fragments fades with observed multiplicities increasing beyond n=30-40, corresponding to estimated actual multiplicities of m=42-63. The reaction yield is taken over by light charged particles and intermediate-mass fragments (IMF). The charge distribution has an approximately exponential character, in agreement with other studies.

In summary of the observations made for the $^{197}Au + ^{208}Pb$ System, the emission patterns of neutrons measured in coincidence with PLFs are characteristic of sequential statistical evaporation from the PLF and TLF. The flow of mass and energy represented in the measured coincident neutrons reflects the relative nuclear motion in the entrance channel. The overall multiplicity of neutrons appears to correlate strongly with reaction features and, hence, provides an excellent indication of the relative magnitude of the collision impact parameter. For the most central collisions, massive PLFs no longer survive. Instead, a significant fraction of the total mass of the system is found disassembled into light-charged particles and small clusters.

3.2 Particle Multiplicity Correlations and Massive-Fragment Production in the Reaction ^{209}Bi + (28.2 MeV/u) ^{136}Xe

A rather complete characterization of collision events has been attempted in the case of the $^{209}Bi + ^{136}Xe$ reaction at a bombarding energy of E_{Lab}/A = 28.2 MeV per nucleon, in an experiment performed at the MSU-NSCL accelerator. In the first of this type of experiment, both light charged particles and neutrons were measured with a detector system covering essentially the full solid angle. Here the Dwarf Ball/Wall detector array[64,65] was placed inside the Rochester NMM,[67] pictured in Fig. 6 (top), together with additional

detector telescopes at forward angles. The following gives a first, rather preliminary account of the data.

In Fig. 14, the charged-product yield measured with a telescope at $\theta = 6^\circ$ ($\theta_g = 7^\circ$) is plotted in form of a logarithmic contour diagram versus atomic number and laboratory energy. Squares and circles result from simulation calculations described further below. The distribution in Fig. 14 shows features similar to those discussed for the reaction $^{197}Au + ^{208}Pb$ (cf. Fig. 8). As an important difference between the two reactions, one notices that PLF fission does not lead to clearly distinguished components, in the case of the $^{209}Bi + ^{136}Xe$ reaction. Massive PLF fragments are seen to be produced with significant cross sections for dissipated energies up to approximately $E_{diss} = 1.5$ GeV representing a value of the order of the kinetic energy above the barrier available in the entrance channel, as estimated from two-body kinematics. In a damped-reaction scenario, this observation would imply that massive PLFs could survive excitation energies of the order of $E^*_{PLF} = 0.7$ GeV without substantial disintegration.

In the $^{209}Bi + ^{136}Xe$ reaction, neutrons, light charged particles, and IMFs are produced with a range of velocities, from smaller to larger than the beam velocity. Fig. 15 provides a sense of the relative multiplicities of neutrons and charged products as functions of excitation energy deposited in the $^{209}Bi + ^{136}Xe$ system. In this figure the measured multiplicity of neutrons, $\langle m_n \rangle$, is plotted versus that of all detected charged particles $\langle m_z \rangle$, in a contour diagram. This $4\pi \times 4\pi$ multiplicity correlation is compatible with the dependence of charged-particle multiplicities on the multiplicity of neutrons, observed[70,71] in single-counter experiments on other systems. The curves in Fig. 15 are results of simulation calculations to be discussed below. The intensity ridge seen in Fig. 15 at $\langle m_n \rangle = 0$ is the result of random triggering in the experiment. At least to a certain extent, the total particle multiplicity must reflect the magnitude of the energy E_{diss} dissipated in a collision. As a consequence, one may interpret the characteristic correlation function exhibited in Fig. 15 to imply that the first 300-400 MeV of excitation energy, generated in

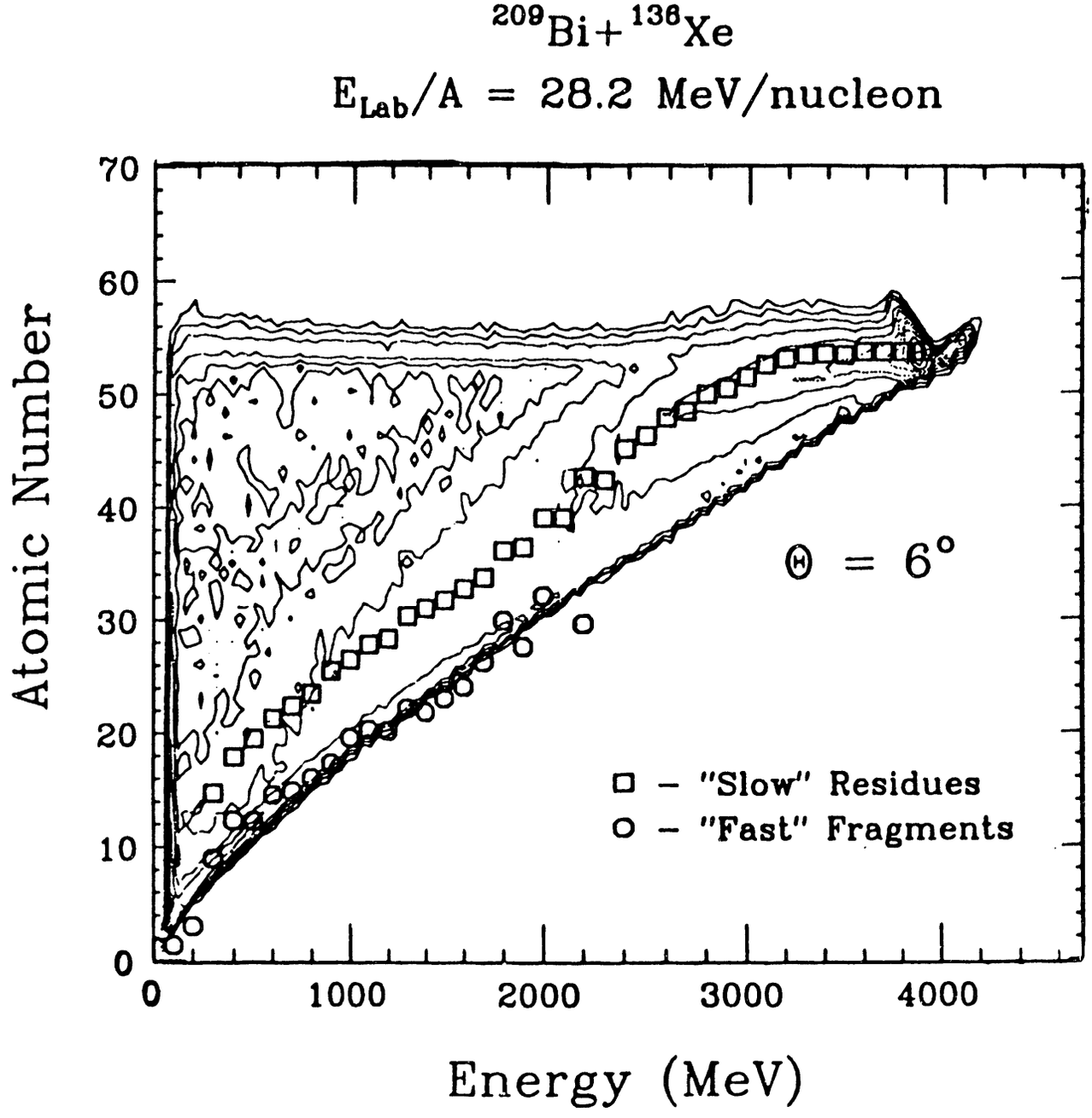
$^{209}Bi + ^{136}Xe$
E_{Lab}/A = 28.2 MeV/nucleon
Atomic Number
Energy (MeV)
Θ = 6°
□ – "Slow" Residues
○ – "Fast" Fragments
0
10
20
30
40
50
60
70
0
1000
2000
3000
4000

Figure 14

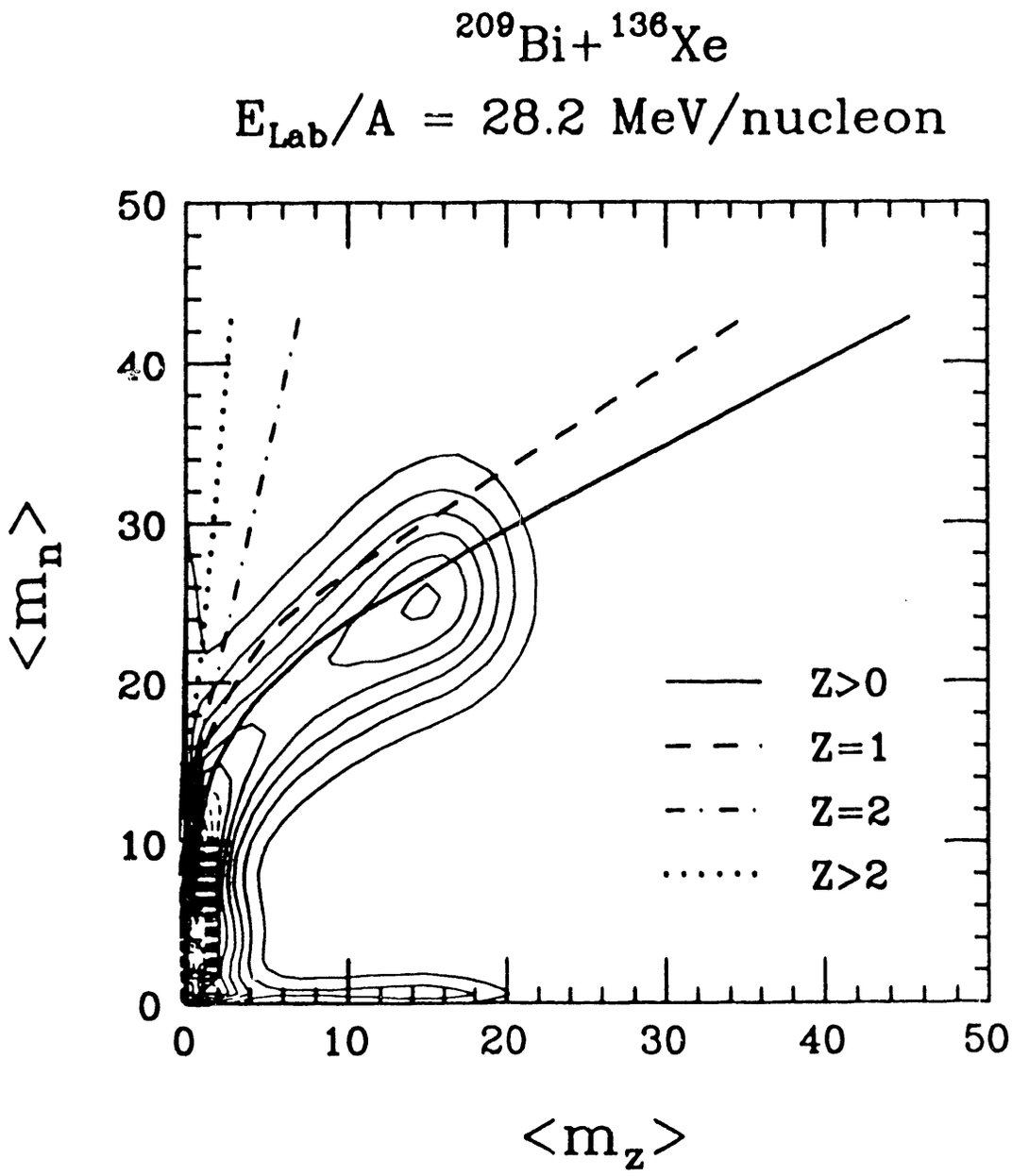
$^{209}Bi+^{136}Xe$
E_{Lab}/A = 28.2 MeV/nucleon
50
40
30
20
10
0
0
10
20
30
40
50
$<m_n>$
$<m_z>$
Z>0
Z=1
Z=2
Z>2

Figure 15

peripheral collisions, lead mainly to the emission of neutrons. Most probable multiplicities of charged particles are approximately zero, for such collisions, increasing to approximately $\langle m_z \rangle = 15$ for central collisions associated with high values of dissipated energy or energy loss. The average number of neutrons observed is approximately equal to $\langle m_n \rangle = 26$, representing an actual number of 58-60 neutrons emitted in a central collision. An approximate account of the average excitation energy carried away per particle deduces temperatures of $\tau \geq 5$ MeV attained by the nuclear system formed in central collisions.

The shape of the multiplicity correlation depicted in Fig. 15, the first measured with full solid-angle coverage, appears to be quite characteristic, although there is no information of this kind for any other reaction to compare with. It seems that the neutron multiplicity is a rather sensitive indicator of the dissipated energy, over the whole range, whereas the charged-particle multiplicity m_z fulfills a similar role only for intermediate to high energy losses, for the present very heavy reaction system. The considerations of the general shape of the neutron multiplicity distribution made in Section 2.2 apply also to the more general case of the two-dimensional multiplicity distribution of Fig. 15. Hence, a peak is expected to occur at high multiplicities. However, somewhat surprisingly, the data show only a rather weak, if any, anticorrelation between the multiplicities m_n and m_z, perhaps partially washed out by the finite resolutions in particle multiplicities.

Correlations between PLF and light particles are illustrated by the contour plots of Fig. 16, where the telescope data of Fig. 14 are displayed in form of a laboratory ΔE-E diagram in the top panel. In the lower two panels of Fig. 16, the yield is plotted versus neutron or light-charged-particle multiplicity, with the abscissa always representing the same laboratory energy E measured with the trigger telescope at $\theta = 6°$. Horizontal and vertical ridges are due to random trigger events. The multiplicities are not corrected for efficiency. With respect to the neutron multiplicity, it is worth remembering (cf. Fig. 6, bottom) that the NMM is much more efficient for neutrons emitted from slow-moving sources such as the TLF. In essence, the middle panel of Fig. 16 displays a correlation

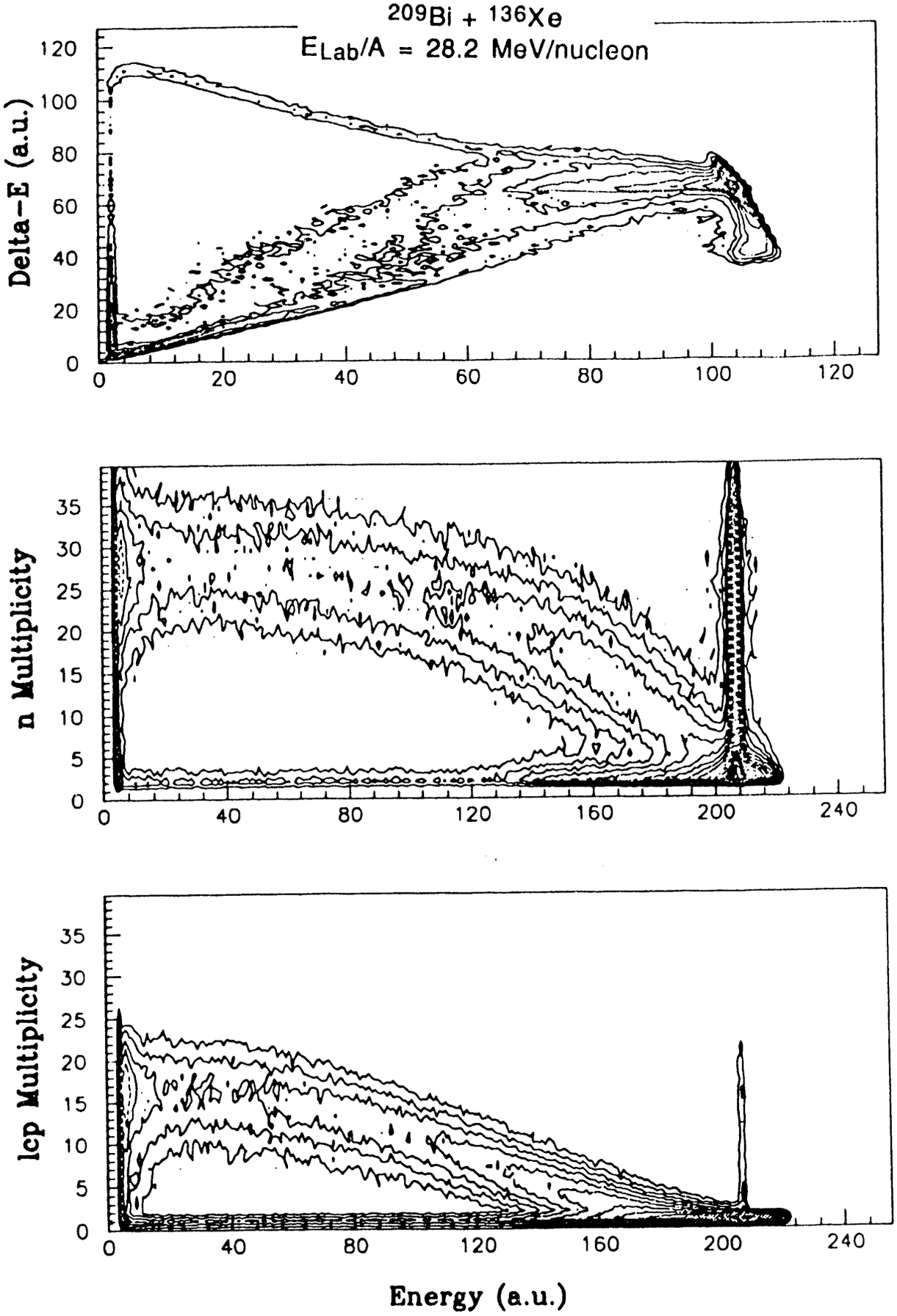
209Bi + 136Xe
ELab/A = 28.2 MeV/nucleon
Delta-E (a.u.)
n Multiplicity
lcp Multiplicity
Energy (a.u.)

Figure 16

between the multiplicity of neutrons emitted from the TLF and the laboratory energy of the PLF reaction partners.

It is apparent from Fig. 16 that the PLF properties such as $\Delta E(Z)$, laboratory energy E, or energy loss correlate quite strongly with the (TLF-) neutron multiplicity, at least for energy losses of up to $\approx$ 2 GeV, i.e., for partially and strongly damped collisions. For events leading to light charged particles or IMFs ($Z \geq 10$) in the telescope, the average neutron multiplicity does not change appreciably with the laboratory energy of the particle. The charged-particle multiplicity (Fig. 16, bottom) exhibits a similar behavior, however, this multiplicity saturates at slightly smaller laboratory E values. It then appears that particle multiplicities increase steadily with decreasing PLF laboratory energy and atomic number (or mass), reflecting increasing amounts of excitation energy deposited in the system. Events leading to relatively small fragments, IMFs, or light charged particles in the telescope are apparently associated with the same strong damping of the initial kinetic energy E_0 above the barrier.

The multiplicity data presented in Fig. 16 have been accumulated under the condition that a charged particle had been registered in the 6° telescope. Conversely, ΔE-E scatter plots for this telescope have been sorted with three coarse conditional gates a), b), c) set on the particle correlation function as defined on the right-hand-side of Fig. 17. The resulting conditional ΔE-E scatterplots are shown on the left-hand-side of that figure. These plots are equivalent to those depicted in Fig. 13 for the $^{197}Au + ^{208}Pb$ reaction discussed earlier. At least for a selected telescope angle, both these data sets demonstrate the presence of strong, monotonic correlations between PLF properties and light-particle multiplicity. Clearly, a low particle multiplicity (gate a)) selects peripheral binary collisions associated with relatively small losses of kinetic energy of a massive PLF, with a large fraction of this dissipated energy deposited in the corresponding TLF. As the multiplicity increases, the PLF kinetic energy and mass (Z) decreases. As in the case of the $^{197}Au + ^{208}Pb$ reaction, the largest multiplicities are associated with central collisions. In such

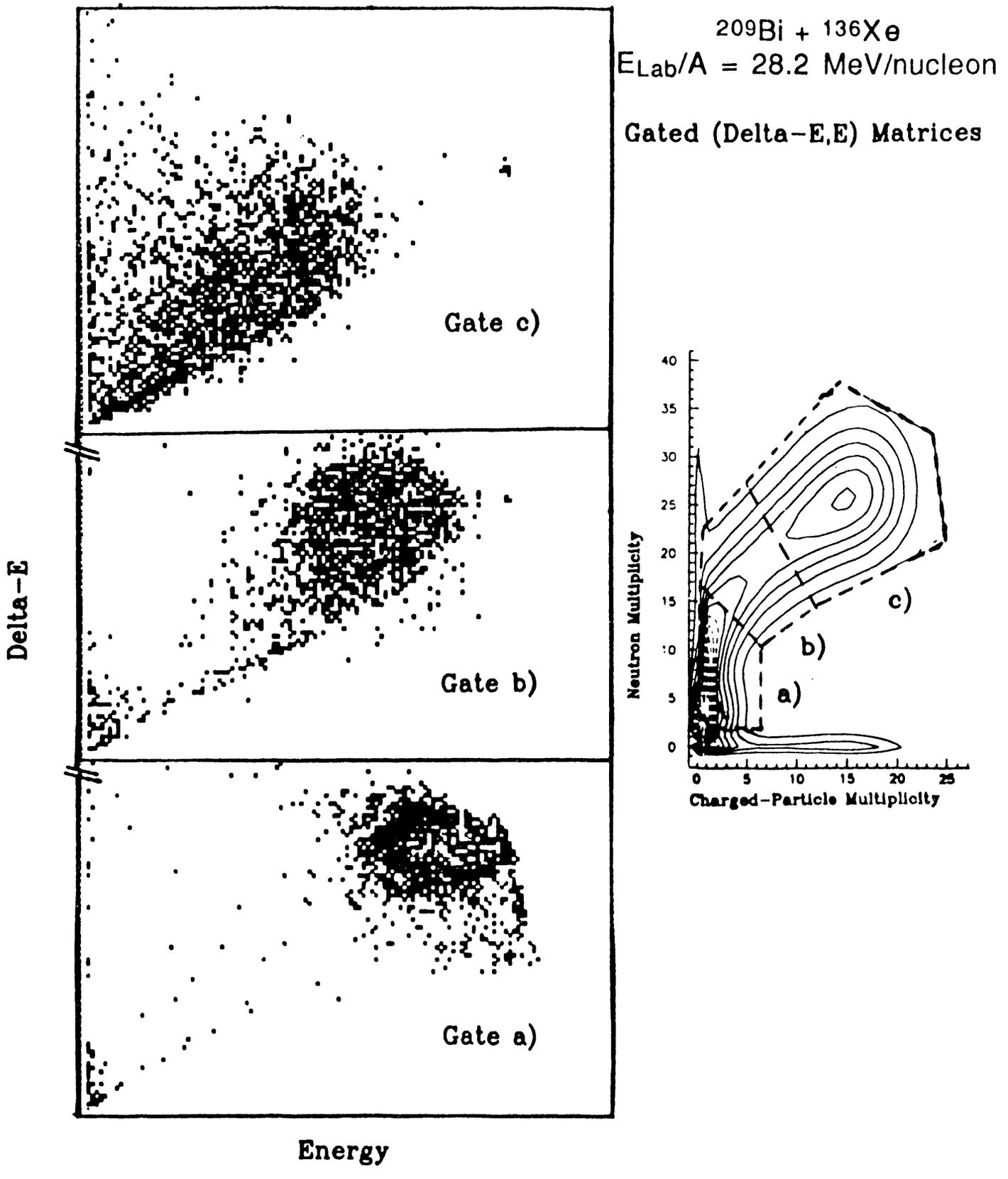
$^{209}Bi + ^{136}Xe$
E_{Lab}/A = 28.2 MeV/nucleon
Gated (Delta-E,E) Matrices
Gate c)
Gate b)
Gate a)
Delta-E
Energy
Neutron Multiplicity
Charged-Particle Multiplicity
a)
b)
c)
0
5
10
15
20
25
30
35
40

Figure 17

collisions, massive PLFs are no longer observed. Possibly, the primary PLFs have acquired enough excitation energy to disassemble into several smaller fragments. Alternatively, the primary process could have been a mononuclear reaction leading to a highly excited nuclear composite that subsequently disintegrates. The preliminary analysis of these data performed to date is not yet able to distinguish unambiguously between these two scenarios, nor does it allow to conclude wether this disintegration is instantaneous or sequential. However, the smooth evolution of all reaction features with total dissipated energy, or energy loss, suggests an equally continuous development of the reaction mechanism with the amount of dissipated kinetic energy.

All the above features appear to be qualitatively consistent with a primary damped reaction mechanism, well-known[1] from the low-energy domain. In the present experiments, the particle multiplicity has apparently taken over the role of the total-kinetic-energy-loss as an indicator of impact parameter and interaction time. It is for these reasons that the data are compared with a simulation calculation based on the one-body theory[4,5] of exchange-induced transport (NEM). Obviously at Fermi energies, some of the assumptions and idealizations made in the model are even less justified than for the lower-energy collisions, for which this model had originally been designed. Calculations of the primary fragment distributions were performed with an NEM code[68] developed earlier. The subsequent decay of representative primary PLF-TLF pairs was modeled with the statistical-model code GEMINI.[72] The response of NMM and charged-particle detector array was approximately taken into account in the calculation of average model correlations that can be compared directly to the data.

The results of such simulation calculations are compared to the experimental fragment and particle multiplicity distributions shown in Figs. 14 and 15, respectively. The NEM predicts a negligible average drift of the fragment charge asymmetry with increasing interaction time, increasing energy loss, and decreasing impact parameter. The evaporation calculation results in no appreciable change in the average atomic numbers of

the PLFs from the primary values for energy losses up to several hundred MeV. This calculation, represented by the open symbols in Fig. 14., reproduces the experimental dependence of the most probable PLF-Z value on laboratory PLF energy E very well. For the first approximately 400 MeV of kinetic-energy loss of the PLF, most of the excitation energy of the PLFs is carried away by sequentially emitted neutrons. For higher excitation energies or energy losses, charged particles are emitted also, reducing the PLF-Z values. For charged-particle laboratory energies below approximately 1.5 - 2 GeV, there are no massive residues of the primary PLFs detected in the telescope. All particles measured in this energy domain result from sequential evaporation from more energetic primary PLFs or their fission, and from the TLFs, according to the calculations.

Because of the high PLF velocity, the kinematics of the evaporated particles are double-valued. Hence, there are two kinematical ridges for PLF-fission fragments, as well as for light charged particles. The data do not show the separated, parallel ridges of cross section predicted by the calculations, possibly because of the neglected width of the fragment distributions. However, the general relation between particle atomic number and laboratory energy is well reproduced by the simulation calculations.

It is then expected that the model also gives a reasonable account of the multiplicity correlations depicted in Fig. 15. Here, the calculations are represented by the solid curve for the correlation between neutrons and any charged particles. The other curves in the figure correspond to various particle atomic numbers Z. The solid curve, representing an average over all charged particles emitted sequentially from damped primary fragments, is seen to reproduce the experimental correlation very well, up to the very high energy losses represented by the the high-multiplicity bump. However, the calculation predicts higher multiplicities for the central collisions than observed. This deficiency could be understood either in terms of incomplete energy deposition which could be limited, e.g., by fast non-statistical particle emission. Alternatively, the higher excitation energies deposited in the intermediate system could lead to enhanced emission of IMFs, a process not well modeled

by the GEMINI code, because of the expected strong increase of nonequilibrium particle multiplicities with decreasing impact parameter and because of the relatively high emission barriers for the IMFs, both processes are expected to affect the correlation in Fig. 15 only for the relatively high neutron multiplicities.

3.3 Particle Evaporation and Nuclear Disassembly in Central Collisions

As has been discussed above, most of the reaction cross section for heavy systems such as those studied here is observed to be consistent with a binary reaction mechanism. However, a significant fraction of the cross section is not associated with massive and fast PLFs. This behavior is demonstrated in the $^{197}Au + ^{208}Pb$ product distribution displayed on the bottom of Fig. 13, and in the top panel of Fig. 17, for the $^{209}Bi + ^{136}Xe$ reaction. The theoretical simulation calculations described in the previous section are not easily adaptable to central collisions in the Fermi energy regime. For example, for the lowest 700 l-waves in the above reaction, amounting to approximately 30% of the total reaction cross section, the model predicts the formation of a highly excited ($\tau \approx 6.4$ MeV) intermediate composite mono-nucleus with a comparatively long lifetime. The decay of such an exotic nuclear system is expected to be rather complex and not tractable with conventional statistical-model codes such as GEMINI. However qualitatively one would expect this nucleus to undergo multiple fission preceded by substantial prescission particle evaporation,[73,74] explaining perhaps the lack of fragments from symmetric fission of the composite system.

Alternative models[8-18] suggest the system formed in central collisions to suffer (instantaneous) multi-fragmentation, vaporization, or explosion. In addition, a statistical-decay model has been proposed[75] for hot, expanding nuclei such as might be produced in central collisions of the heavy systems studied in this work. This latter model predicts several IMFs to be produced sequentially in central collisions of somewhat lighter systems. While calculations for the present two systems are not yet available, the preliminary results

of the particle multiplicity correlations summarized in Fig. 15 are consistent with a significant IMF yield in central collisions.

A significant IMF yield could represent the signature of a novel deexcitation or disassembly process. The kinetic energies of these particles limit the amount of energy available for intrinsic fragment excitation. Most of the thermal excitation energy introduced into a heavy system and its complex decay products is eventually carried off by evaporated neutrons and, to a lesser extent, by light charged particles. A summary of the most probable neutron multiplicities measured in central collisions is displayed in Fig. 18. Here, the multiplicity corresponding to the peak of the "central-collision bump" of the neutron multiplicity distribution (cf. Fig. 12) is plotted versus the mass number of the target nucleus, as measured in reactions induced by 28-MeV/u ^{136}Xe, 45-MeV/u ^{132}Xe, and 29-MeV/u ^{208}Pb projectiles. The multiplicities are not corrected for efficiency, but the ^{136}Xe point has been scaled by the ratio of the efficiencies of the two different NMM devices used in the measurements.

The general trends of the systematics of Fig. 18 are rather clear. The multiplicities increase with the masses of both projectile and target. In addition, a given multiplicity of neutrons is produced in a central collision of a heavy system at a lower bombarding energy per nucleon than for a lighter system. The effect could simply be due to a larger number of neutrons present in a heavier system and the corresponding low Q-values for neutrons, favoring neutron emission over other decay channels even at high temperatures. Alternatively, it could reflect generally higher temperatures attained by these heavier systems. Both situations are compatible with Fig. 19, where the average fraction of all neutrons of a system emitted in a central collision is plotted versus this total number, for various reaction systems, all measured at a bombarding energy of about 30 MeV/u. Although the fraction of all neutrons emitted by a heavy composite system can be significant, most of the neutrons are still bound in charged reaction products. Nevertheless, the systematics depicted in Figs. 17 and 18 provide important constraints on

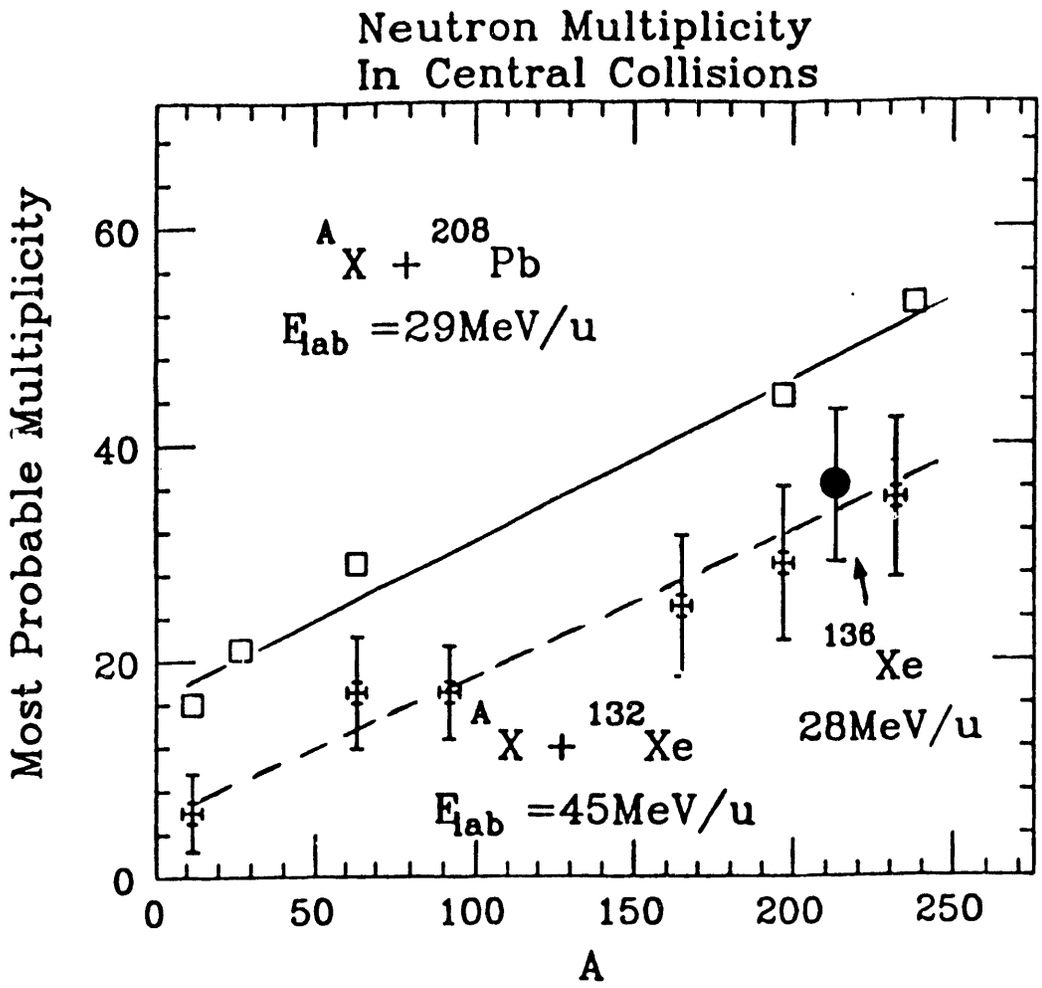
Neutron Multiplicity
In Central Collisions
Most Probable Multiplicity
A X + 208 Pb
E lab =29MeV/u
136 Xe
28MeV/u
A X + 132 Xe
E lab =45MeV/u
0
20
40
60
0
50
100
150
200
250
A

Figure 18

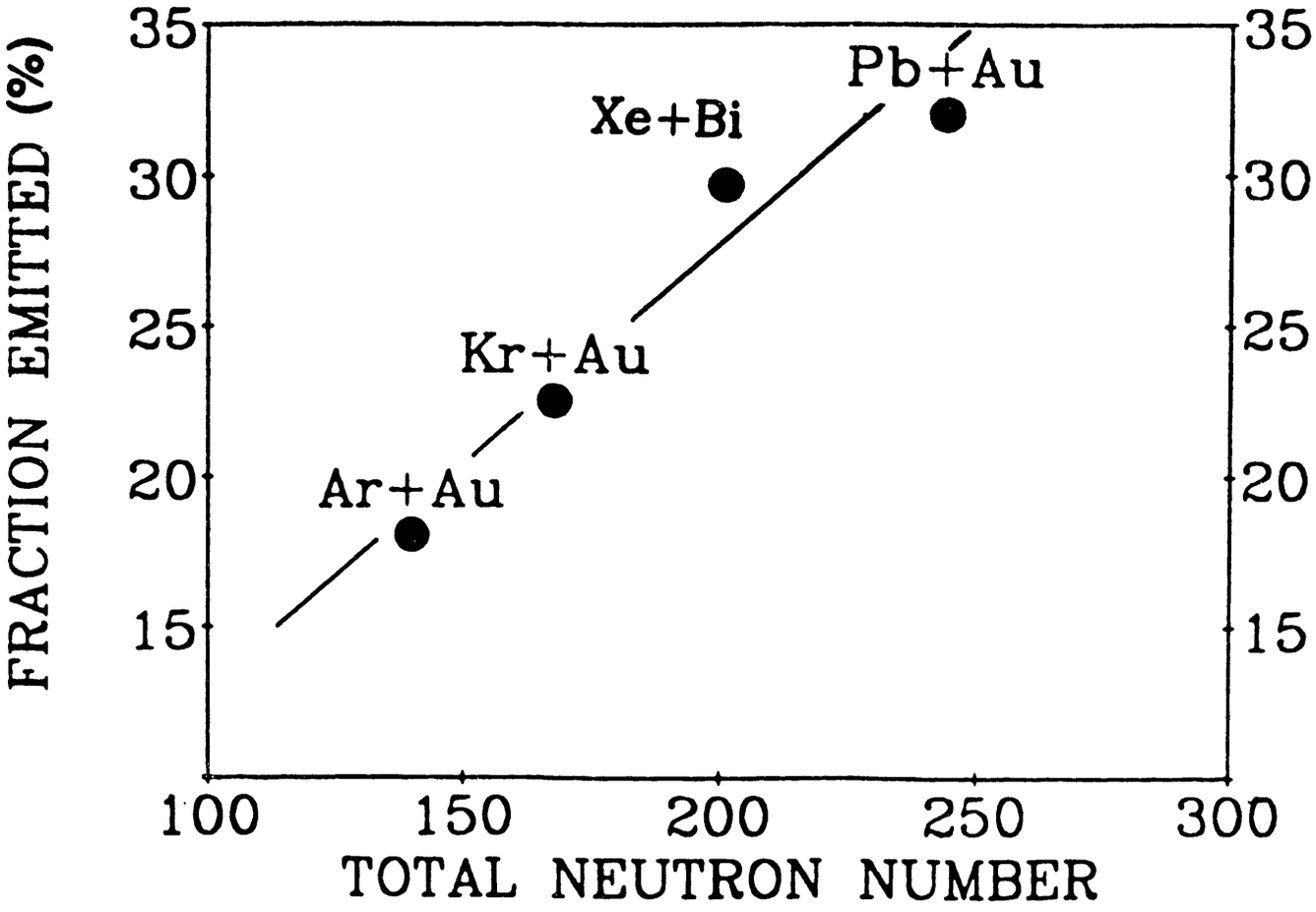
FRACTION EMITTED (%)
35
30
25
20
15
Pb+Au
Xe+Bi
Kr+Au
Ar+Au
100
150
200
250
300
TOTAL NEUTRON NUMBER

Figure 19

reaction models, together with the broad distributions of light particles and clusters produced in central collisions.

4. CONCLUSIONS

In summary, it was found in the studies of heavy-ion reactions between 15 and 30 MeV/u presented here, that the basic reaction mechanism develops in a very smooth fashion, with binary damped reactions probably still dominating at least for intermediate and large impact parameter, accounting for roughly 70% of the reaction cross section, in the case of a heavy system such as ^{209}Bi + ^{136}Xe at 28.2 MeV/u. This conclusion is based on the characteristic correlations found between the amount of dissipated energy, measured via the multiplicity of neutrons emitted mainly by the TLF, and the properties of the PLF. In the case of the ^{209}Bi + ^{136}Xe reaction, a transport model calculation based on the NEM combined with an evaporation code provides a quantitative reproduction of the correlation between neutrons and charged particles and that between PLF laboratory energy and atomic number. However, this model overestimates the number of light particles and neutrons emitted in central collisions, but underestimates the yield of more complex IMFs.

In agreement with earlier studies both at low and intermediate energies, it was found in this work that the neutron multiplicity is an excellent indicator of the ℓ-value or impact parameter of a collision. The neutron multiplicity assumes the role of the energy loss parameter used extensively in reaction studies at lower bombarding energies. The multiplicity of light charged particles also provides a measure of the impact parameter. However, for heavy systems, this observable is sensitive only in the range from low to intermediate impact parameter. It is expected that the roles of neutrons and light charged particles are interchanged for light reaction systems.

The persistence of the damped binary reaction mechanism at Fermi energies and the smooth evolution of the observed reaction features with impact parameter suggest that the disappearance of massive PLFs in central collisions is most likely due to sequential disintegration of the hot intermediate mononuclear or dinuclear system. At least in the

present study, there is no conclusive evidence found for an instantaneous multifragmentation. Higher intrinsic excitation energies may be required to trigger such a disintegration process. Such critical temperatures may be difficult to reach, if the systematics of preequilibrium particle emission, leading to a fast cooling of the system, can be extrapolated linearly to higher bombarding energies. More data are needed to settle this important question.

Acknowledgement

The data presented in this article are due to the efforts of several collaborations. The teams of Refs. 49 and 61 generated the data on the $^{197}Au + ^{208}Pb$ system, while the preliminary results on the reaction $^{209}Bi + ^{136}Xe$ have been obtained by S.P. Baldwin, B. Lott, B.M. Quednau, B.M. Szabo, W.U. Schröder, and J. Tõke (Univ. of Rochester), R.T. de Souza (MSU), J.G. Barreto, R. Charity, L. Gallamore, D.G. Sarantites, and L.G. Sobotka (Washington Univ.)

The authors is grateful to Dr. R.C. Block and the Rensselaer Polytechnique Institute for the donation of the original hardware of the Rochester NMM.

This work was supported by the U.S. Department of Energy under grant number DE-FG02-88ER40414.

References

1. W.U. Schröder et al., in "Treatise on Heavy-Ion Science," Vol. 2, p. 113, D.A. Bromley, Editor, Plenum Press, New York and London, 1984, and references cited therein.

2. R.G. Stokstad, in "Treatise on Heavy-Ion Science," Vol. 2, p. 81, D.A. Bromley, Editor, Plenum Press, New York and London, 1984, and references cited therein.

3. Ch. Ngô, *Progr. Part. Nucl. Phys.* **16** (1986) 139 and references cited therein.

4. J. Randrup, *Nucl. Phys.* **A307** (1978) 319; A327 (1979) 490; A383 (1982) 468.

5. J. Døssing et al., *Nucl. Phys.* **A433** (1985) 215; A433 (1985) 280.

6. L. Tassan-Got, Ph.D. thesis, Orsay 1988, Report IPNO-T-89-02, IPNO-DRE-89-46.

7. D. Pade et al., *Phys. Rev.* C**43** (1991) 1288.

8. C. Gregoire and B. Tamain, *Ann. Phys. Fr.* **11** (1986) 323 and references cited therein.

9. C.K. Gelbke and D.H. Boal, *Progr. Part. Nucl. Phys.* **19** (1987) 33, and references cited therein.

10. G.F. Bertsch et al, *Phys. Rep.* **160** (1988) 189, and references cited therein.

11. J. Aichelin, et al., *Phys. Lett.* **163B** (1985) 59.

12. J. Aichelin, et al., *Phys. Rev.* C**33** (1986) 537.

13. G. Fai et al., *Nucl. Phys.* A**404** (1983) 551; *Nucl. Phys.* A**381** (1982) 557.

14. J.P. Bondorf et al., *Nucl. Phys.* A**443** (1985) 321.

15. D.H.E. Gross et al., *Phys. Rev. Lett.* **56** (1986) 1544, *Nucl. Phys.* A**461** (1987) 641; A**461** (1987) 668, and *Phys. Rep.* to be published.

16. J.A. López et al., *Nucl. Phys.* A**503** (1989) 183; ibid., A**512** (1990) 345.

17. E. Suraud, *Nucl. Phys.* **462** (1987) 109; Proc. Symp. Nucl. Dyn. Nucl. Disassembly, J.B. Natowitz, editor, (World Scientific, Singapore, 1989), p 464.

18. B. Borderie et al., *Ann. Phys.* (Fr) **15** (1990) 287.

19. A.S. Goldhaber, *Phys. Lett.* B**53** (1974) 306.

20. J. Hüfner, Proc. 4th High-Energy Heavy-Ion Summer Study Berkeley 1978, Report LBL-7766, p. 135.

21. W.A. Friedman, *Phys. Rev.* C**27** (1983) 569.

22. A. Bonasera et al., *Nucl. Phys.* A**463** (1987) 653.

23. S. Levit and P. Bonche, *Nucl. Phys.* A**462** (1987) 109.

24. E. Suraud, Proc. Symp. Nucl. Dyn. Nucl. Disassembly, J.B. Natowitz, editor, (World Scientific 1989) p. 464.

25. F. Rami et al., *Z. Physik* A**318** (1984) 239.

26. D. Guerreau, *Nucl. Phys.* A**442** (1985) 37C.

27. R. Dayras et al., *Nucl. Phys.* A**460** (1986) 299.

28. G. Rudolf et al., Proc. Symp. Nucl. Dyn. Nucl. Disassembly, J.B. Natowitz, editor, (World Scientific 1989) p. 170.

29. D. Guerreau, in Nuclear Matter and Heavy-Ion Collisions, M. Soyer, H. Flocard, B. Tamain, and M. Porneuf, editors, (Plenum Publ. Corp., 1989) p. 187.

30. J. Galin, Proc. Symp. Nucl. Dyn. Nucl. Disassembly, J.B. Natowitz, editor, (World Scientific 1989) p. 320.

31. J. Wile et al., *Phys. Rev. Lett.* **63** (1989) 2551.

32. J.R. Huizenga et al., *Phys. Rev. Lett.* **37** (1976) 885.

33. V.E. Viola et al., *Phys. Rev.* C**31** (1985) 1550.

34. T.C. Awes et al., *Phys. Rev. Lett.* **52** (1984) 251.

35. R. Vandenbosch et al., *Phys. Rev. Lett.* **52** (1984) 1964.

36. H. Sohlbach et al., *Phys. Lett.* B**153** (1985) 386; *Nucl. Phys.* A**467** (1987) 349; *Z. Phys.* A**328** (1987) 205.

37. L.G. Sobotka et al., *Phys. Lett.* B**175** (1986) 27.

38. J.A. Wile et al., *Phys. Rev.* C**35** (1987) 1608; *Phys. Rev.* C**40** (1989) 1700.

39. J. Tõke et al., *Phys. Rev.* C**43**, 1991.

40. W.U. Schröder et al., *Phys. Rev.* C**16** (1977) 623.

41. D. Hilscher et al., Proc. Workshop Coinc. Part. Emission Cont. States, Bad Honnef 1984, (World Scientific, Singapore, 1984) p. 268.

42. E. Holub et al., *Phys. Rev.* C**33** (1986) 143.

43. J. Péter et al., *Phys. Lett.* B**237** (1990) 187.

44. M. Conjeaud et al., *Phys. Lett.* B**159** (1985) 244.

45. U. Jahnke et al., Proc. XX International Summer School Nucl. Phys., Mikolajki, 1988, Report HMI-B 463, 1988.

46. M. Blann, *Ann. Rev. Nucl. Sci.* **15** (1975) 123.

47. M. Blann, *Phys. Rev.* C**23** (1981) 205; ibid. **31** (1985) 1245.

48. H. Machner, *Z. Physik* A**321** (1985) 577.

49. B.M. Quednau et al., Proc. VII Workshop Nucl. Dynamics, Key West 1991 (World Scientific), in press.

50. J.P. Bondorf et al., *Nucl. Phys.* A**333** (1980) 285.

51. M.C. Robel, Ph.D. thesis, Lawrence Berkeley Laboratory preprint LBL-8181 (1979), unpublished.

52. J. Randrup and R. Vandenbosch, *Nucl. Phys.* A**474** (1987) 219.

53. D. Hilscher et al., *Phys. Rev.* C**20** (1980) 576.

54. J.L. Wile et al., *Phys. Rev.* C**35** (1987) 1608.

55. W.U. Schröder, Nucl. Sci. Res. Conf. Ser. Vol 2 (1980) 19.

56. B.C. Diven et al., *Phys. Rev.* **109** (1958) 144, ibid. **120** (1960) 556.

57. J. Poitou et al., *Nucl. Inst. Meth.* **114** (1974) 113.

58. U. Jahnke et al., Lecture Notes in Physics 178, (Springer, Berlin 1983), p. 179.

59. B.M. Quednau et al., Report DOE/ER/40414-2, (W.U. Schröder, J.R. Huizenga, editors), p. 170, unpublished.

60. J. Galin et al., Proc. Symp. Heavy-Ion Coll. Obernai 1990, World Scientific, in press.

61. E. Piasecki et al., *Phys. Rev. Lett* **66** (1991) 1291.

62. M. Morjean et al., Proc. VII Workshop Nucl. Dyn., Key West 1991, World Scientific, in press.

63. D. Jacquet et al., Proc. XXIX Int. Winter Meeting Nucl. Phys., Bormio 1991, in press.

64. D.G. Sarantites et al., *Nucl. Inst. Meth.* A**264**, 319 (1988).

65. E. Norbeck et al., *Nucl. Inst. Meth.* A**262** (1987) 546.

66. S.P. Baldwin et al., this report and to be published

67. S.P. Baldwin et al., Report DOE/ER/40414-3, (W.U. Schröder and J.R. Huizenga, editors) 1990, p. 247.

68. W.U. Schröder et al., Nucl. Sci. Res. Conf. Ser. Vol. II, (1987) p. 255.

69. A. Pantaleo et al., *Nucl. Inst. Meth.* A**269** (1988) 580.

70. D.X. Jiang et al., *Nucl. Phys.* A**503** (1989) 560.

71. A. Sokolov, These de Doctorat, Universite Paris 6, Report GANIL T9001, 1990.

72. R.J. Charity et al., *Nucl. Phys.* A**483** (1988) 371.

73. D. Hilscher et al., *Phys. Rev. Lett.* **62** (1989) 1099.

74. D. Hinde et al., *Nucl. Phys.* A**502** (1989) 497c.

75. W.A. Friedman, *Phys. Rev. Lett.* **60** (1988) 2125.

DISCLAIMER

This report was prepared as an account of work sponsored by an agency of the United States Government. Neither the United States Government nor any agency thereof, nor any of their employees, makes any warranty, express or implied, or assumes any legal liability or responsibility for the accuracy, completeness, or usefulness of any information, apparatus, product, or process disclosed, or represents that its use would not infringe privately owned rights. Reference herein to any specific commercial product, process, or service by trade name, trademark, manufacturer, or otherwise does not necessarily constitute or imply its endorsement, recommendation, or favoring by the United States Government or any agency thereof. The views and opinions of authors expressed herein do not necessarily state or reflect those of the United States Government or any agency thereof.

END

DATE
FILMED
1 / 26 / 91